# A stress-dependent TRIM28–ALKBH2 feedback loop modulates chemotherapy response

Zhiming Sun[1], Yunfang Deng[1], Yue Liu[1], Zhaohui Liu[1], Jiabing Li[1], Lihui Wu[1], Liyuan Zeng[1], Xiaorong Feng[1], Lin Miao[1], Ying Sheng[1], Bei Chen[1], Yuming He[1], Ye Liu[1] & Yu Zhao[1,2]*

[1]The National & Local Joint Engineering Laboratory of Animal Peptide Drug Development, College of Life Sciences, Hunan Normal University, Changsha, Hunan, 410081, China

[2]Peptide and Small Molecule Drug R&D Platform, Furong Laboratory, Hunan Normal University, Changsha, Hunan, 410081, China

* Corresponding author: Yu Zhao (smile_zhao@hotmail.com)

Running title: TRIM28–ALKBH2 modulates chemoresistance

***Keywords***: TRIM28, ALKBH2, MAGEA6, Ubiquitination, Chemoresistance

**ABSTRACT**

Chemoresistance to DNA-damaging agents, including platinum and alkylating compounds, limits treatment efficacy in non-small cell lung cancer (NSCLC) and is frequently associated with elevated DNA repair activity. Here, we identify a stress-responsive feedback loop between the E3 ligase TRIM28 and the demethylase ALKBH2. TRIM28 directly binds ALKBH2 and mediates its K48-linked polyubiquitination and proteasomal degradation, whereas ALKBH2 enhances TRIM28 transcription, forming a reciprocal loop that regulates their steady-state levels. Alkylation stress triggers a biphasic response: acute MMS exposure increases TRIM28–ALKBH2 complex formation, further augmented by MAGEA6, and accelerates ALKBH2 degradation, whereas prolonged MMS treatment induces K48-linked ubiquitination and proteasomal degradation of TRIM28, leading to ALKBH2 stabilization and increased ALKBH2 transcription. Clinically, ALKBH2 is elevated in lung adenocarcinoma and correlates with poorer survival, whereas TRIM28 shows prognostic association only in chemotherapy-treated patients. Functionally, combining MMS with cisplatin increases DNA damage, reduces clonogenic survival, and attenuates ALKBH2-dependent tolerance to alkylation damage, linking the TRIM28–ALKBH2 axis to chemotherapy response in NSCLC. Together, these results identify a stress-responsive biphasic TRIM28–ALKBH2 regulatory loop that coordinates ubiquitin-dependent and transcription-linked mechanisms to shape alkylation responses and modulate chemotherapy sensitivity in NSCLC.

## Introduction

Cells are continuously exposed to endogenous metabolites and environmental or therapeutic alkylating agents that generate cytotoxic and mutagenic DNA adducts, thereby threatening genome integrity[1,2]. These lesions are repaired through three principal mechanisms: base excision repair (BER), direct reversal by $O^6$-methylguanine-DNA methyltransferase (MGMT), and oxidative demethylation catalyzed by AlkB family of Fe(II)/α-ketoglutarate–dependent dioxygenases[3-5]. AlkB enzymes remove N-linked methyl lesions such as 1-meA and 3-meC through a coupled oxidative reaction that restores the native base[6-8]. In mammalian cells, these dioxygenases operate alongside BER and MGMT to resolve lesions that evade other pathways, supporting genome maintenance across diverse cellular conditions. Accordingly, changes in AlkB enzyme expression or stability correlate with distinct cellular responses to alkylation damage, indicating the importance of precise control over this pathway.

In addition to transcriptional and epigenetic regulation[9-13], the protein levels of AlkB family dioxygenases are controlled by ubiquitin-dependent proteostasis mechanisms. Extensive studies have characterized ubiquitin-regulatory networks for several homologues, most notably FTO and ALKBH5. FTO turnover is controlled by multiple context-dependent E3 ligases—including TRIM17, DTX2, MIB1, and RNF144A—and is further modulated by TRIM21 following O-GlcNAc–primed modification[14-18]. ALKBH5 stability is similarly regulated by RNF180 or by PRMT5-dependent methylation that promotes its recognition by TRIM28[19,20]. These degradative pathways are counterbalanced by substrate-specific deubiquitinases (DUBs), including USP7 and USP18 for FTO[21,22], and USP14 and USP36 for ALKBH5[23,24]. OTUD4 has also been reported to stabilize the related demethylase ALKBH3 through a scaffolding DUB mechanism[2], consistent with the broader reliance of AlkB-family enzymes on ubiquitin-dependent regulation.

Among the nine mammalian AlkB homologues, ALKBH2 is the principal demethylase that repairs methylated bases in duplex DNA and plays a central role in suppressing alkylation-induced mutagenesis[25-28]. ALKBH2 is frequently upregulated in cancer, particularly in non–small cell lung cancer (NSCLC), where elevated expression is associated with increased tolerance to DNA

damage and reduced responsiveness to alkylating or platinum-based chemotherapy[11,27,29-31]. Because alkylating chemotherapeutics such as temozolomide and environmental exposures such as cigarette smoke generate similar methylated lesions[1,32,33], tight control of ALKBH2 protein levels is important for tumor survival under sustained alkylation stress[11,34]. However, the ubiquitin-dependent mechanisms regulating ALKBH2 stability—including whether it undergoes ubiquitination and the identity of any responsible E3 ligases or DUBs—remain poorly defined. Notably, the ALKBH2-associated ASCC complex recruits TRIM28 upon MMS-induced alkylation stress[35], placing TRIM28 within the alkylation repair environment and raising the possibility of a regulatory connection between TRIM28 and ALKBH2.

The tripartite motif (TRIM) family of RING-type E3 ligases—including TRIM28 and TRIM24—coordinates ubiquitin signaling that integrates chromatin regulation with cellular stress responses[36-38]. TRIM28 uses its N-terminal RING domain and C-terminal PHD–BRD module to mediate KRAB-ZNF–dependent transcriptional silencing and maintain genomic stability[39,40]. Although TRIM28 functions as a key corepressor and E3 ligase, its own activity and availability are tightly regulated at multiple levels. In response to DNA double-strand breaks, TRIM28 undergoes ATM/ATR-dependent phosphorylation at Ser824 to relax heterochromatin and enable repair factor recruitment[41-43]. Its expression is further shaped by transcriptional programs (e.g., NR3C2), post-transcriptional control via NSUN2-mediated $m^5C$ modification or stabilization by the lncRNA PITAR[44-46], and ubiquitin-dependent turnover mediated by RNF4 during genotoxic stress or by March5 under metabolic stress[47,48]. Moreover, MAGE family proteins—including MAGEA6—serve as cofactors that facilitate TRIM28 recruitment to its substrates by promoting assembly of TRIM28–substrate E3 complexes[49-51]. This scaffolding function positions MAGE proteins as modulators of TRIM28-dependent ubiquitin signaling. Despite this multi-layered regulation, how TRIM28 interfaces with alkylation repair pathways, particularly in response to alkylating stress, remains poorly defined.

In this study, we identify an unrecognized regulatory axis involving TRIM28, MAGEA6, and ALKBH2 that becomes functionally engaged under alkylation stress. This feedback loop links

91 TRIM28-dependent ubiquitination of ALKBH2 with ALKBH2-mediated transcriptional
92 regulation of TRIM28, forming a basal loop that is subsequently reprogrammed by alkylation
93 damage. Remarkably, alkylation stress triggers a biphasic regulatory shift—an early phase in
94 which TRIM28–ALKBH2 association increases and ALKBH2 degradation accelerates, followed
95 by a later phase marked by TRIM28 degradation, ALKBH2 stabilization, and transcriptional
96 upregulation. This regulatory architecture integrates ubiquitin-dependent regulation with
97 demethylation repair in a time-dependent manner, providing a mechanistic basis for how the
98 duration of alkylation stress shapes repair capacity and chemotherapy sensitivity in NSCLC.

## Results

### TRIM28 directly binds ALKBH2

To identify proteins associated with TRIM28, we performed tandem affinity purification in H1299 non–small cell lung cancer (NSCLC) cells, followed by silver staining and LC–MS/MS. This analysis identified ALKBH2 as a candidate interactor (Fig. 1A, Supplementary Fig. 1A, Supplementary Table 1). Co-immunoprecipitation (co-IP) in HEK293T cells co-expressing HA-tagged ALKBH2 and Flag-tagged TRIM28 confirmed this association, whereas the related paralog TRIM24 showed no detectable interaction (Fig. 1B). Reciprocal co-IP using HA-ALKBH2 further validated the interaction (Fig. 1C). Domain mapping using TRIM28 truncation mutants indicated that the BCC region (B-box + coiled-coil; residues 141–400) was required for ALKBH2 binding (Fig. 1D, E). Endogenous co-IP in H1299 cells detected ALKBH2 in TRIM28 immunoprecipitates (Fig. 1F), and immunofluorescence analysis revealed their nuclear co-localization (Fig. 1G).

*In vitro* MBP pull-down assays using purified recombinant proteins showed that TRIM28 directly binds ALKBH2 (Fig. 1H). Specificity assays revealed stronger binding to ALKBH2 than to ALKBH3 (Fig. 1I) or the direct-reversal repair enzyme MGMT (Supplementary Fig. 1B). Protein–protein docking predicted a TRIM28–ALKBH2 interface that overlaps the nucleic-acid-binding region of ALKBH2, centered on the Finger (hairpin) motif and the flexible Long-loop[52], which are present in ALKBH2 but absent in ALKBH3 (Fig. 1J). Consistent with this model, single-stranded DNA (ssDNA) competitively reduced TRIM28–ALKBH2 binding in a dose-dependent manner (Fig. 1K), a commonly used approach to assess the DNA-occupied states of repair enzymes [53,54]. Collectively, these data indicate that TRIM28 directly binds ALKBH2 through its BCC domain and support a model in which DNA binding limits TRIM28 access to the ALKBH2 interaction interface.

### A reciprocal TRIM28–ALKBH2 regulatory loop coordinates ALKBH2 ubiquitination and stability, with ALKBH2 enhancing TRIM28 transcription

125 To determine whether ALKBH2 undergoes ubiquitin-dependent modification, we performed
126 denaturing immunoprecipitation (IP) of Flag-ALKBH2 from HEK293T cells co-transfected with
127 HA-ubiquitin (Ub). A high-molecular-weight smear corresponding to polyubiquitinated ALKBH2
128 was detected, which increased markedly after proteasome inhibition with MG132 (Fig. 2A).
129 Expression of a K48-only ubiquitin mutant further enhanced ALKBH2 ubiquitination, whereas the
130 K48R mutant almost completely abolished it (Fig. 2B), indicating that ALKBH2 is predominantly
131 modified by K48-linked polyubiquitin chains. Halo-TUBE pull-down assays revealed that
132 ALKBH2 undergoes endogenous K48-linked polyubiquitination (Fig. 2C).

133 We next examined whether TRIM28 mediates this modification. Overexpression of wild-type
134 (WT) TRIM28 increased K48-linked ubiquitination of ALKBH2 (Fig. 2D), whereas the RING-
135 inactive C65/68A mutant (previously shown to abolish TRIM28 E3 ligase activity[50]) did not
136 increase this modification (Fig. 2F). TRIM28 depletion using two independent shRNAs markedly
137 reduced ALKBH2 ubiquitination (Supplementary Fig. 2A), and re-expression of shRNA-resistant
138 WT TRIM28 restored this activity (Fig. 2E). These data indicate that TRIM28 E3 ligase activity
139 is required for efficient K48-linked ubiquitination of ALKBH2.

140 We then assessed how this modification affects ALKBH2 protein stability. TRIM28
141 knockdown in H1299 and A549 cells increased ALKBH2 protein levels without altering its mRNA
142 expression (Fig. 2G, H), and similar results were obtained after CRISPR/Cas9-mediated TRIM28
143 depletion (Supplementary Fig. 2B). Cycloheximide (CHX) chase assays revealed that TRIM28
144 knockout extended ALKBH2 half-life, whereas TRIM28 overexpression shortened it in a RING-
145 dependent manner (Supplementary Fig. 2C-F). Increasing TRIM28 expression produced a dose-
146 dependent decrease in ALKBH2 protein level in both H1299 and HEK293T cells (Fig. 2I). These
147 data indicate that TRIM28 limits ALKBH2 protein levels by promoting proteasome-mediated
148 degradation (Supplementary Fig. 2G).

149 To determine whether ALKBH2 in turn regulates its E3 ligase, we depleted ALKBH2 in
150 H1299 cells using two independent shRNAs. TRIM28 protein levels were reduced following
151 ALKBH2 knockdown (Fig. 2J), and re-expression of Flag-ALKBH2 restored TRIM28 protein

152 levels (Fig. 2K). ALKBH2 overexpression increased TRIM28 mRNA as measured by qRT-PCR
153 (Fig. 2L). Consistent with this regulatory relationship, TCGA lung adenocarcinoma data indicate
154 that ALKBH2 and TRIM28 transcripts are positively correlated (Supplementary Fig. 2H).
155 Collectively, these data indicate a reciprocal regulatory loop in which TRIM28 promotes K48-
156 linked ubiquitination and proteasome-dependent degradation of ALKBH2, whereas ALKBH2
157 increases TRIM28 expression at the transcriptional level.
158

159 **MAGEA6 enhances TRIM28 E3 ligase assembly and activity toward ALKBH2, a function**
160 **impaired by cancer-associated variants**

161 MAGE family proteins interact with TRIM-type E3 ligases to modulate their activity[50,55]. We
162 therefore examined how MAGEA6 contributes to the organization of the TRIM28–ALKBH2
163 complex. Co-IP in HEK293T cells showed that MAGEA6 binds ALKBH2 (Fig. 3A), and pull-
164 down assays with purified proteins confirmed that this interaction is direct (Fig. 3B). TRIM28
165 depletion did not disrupt MAGEA6–ALKBH2 binding (Fig. 3C), indicating that MAGEA6
166 engages ALKBH2 independently of TRIM28. Rather than serving solely as a TRIM28 scaffold,
167 MAGEA6 directly interacts with ALKBH2 and enhances assembly of the TRIM28–ALKBH2
168 complex. In line with this, Myc-MAGEA6 overexpression increased TRIM28–ALKBH2
169 association in a dose-dependent manner (Fig. 3D, Supplementary Fig. 3A), whereas knockdown
170 of endogenous MAGEA3/6—detected together owing to 96% sequence identity[56]—reduced this
171 interaction (Fig. 3E). The related protein MAGEC2 similarly enhanced TRIM28–ALKBH2
172 assembly (Supplementary Fig. 3B), supporting a conserved function within the MAGEA/C
173 subfamily.

174 To determine the functional consequence of this stabilized complex, we examined its impact
175 on ALKBH2 ubiquitination and turnover. MAGEA6 knockdown reduced endogenous ALKBH2
176 ubiquitination, and re-expression of MAGEA6 restored it (Supplementary Fig. 3C). Conversely,
177 MAGEA6 overexpression promoted K48-linked ubiquitination of ALKBH2, whereas this effect
178 was abolished by TRIM28 knockdown, indicating that MAGEA6 requires TRIM28 to enhance

179 ALKBH2 ubiquitination (Fig. 3F). Accordingly, MAGEA6 accelerated ALKBH2 degradation in
180 control cells, but not in TRIM28-knockout H1299 cells (Fig. 3G, H).

181 MAGEA6 mutations have been reported across cancer types, including lung cancer[57]. To test
182 whether such variants disrupt this regulatory module, we sequenced endogenous MAGEA6 cDNA
183 from H1299 cells and identified two variants, MutA and MutB, carrying 12 and 20 amino-acid
184 substitutions, respectively (Supplementary Fig. 3D). Both mutants were cloned and sequence-
185 verified. Co-IP assays showed that MutA and MutB exhibited reduced binding to ALKBH2, and
186 MutB also showed decreased interaction with TRIM28 (Fig. 3I). Consistent with these defects,
187 both variants displayed impaired promotion of ALKBH2 ubiquitination and degradation relative
188 to wild-type MAGEA6 (Fig. 3J, Supplementary Fig. 3E).

189 To further define the structural basis of this interaction, AlphaFold3 modeling predicted a
190 TRIM28-contacting interface within the MAGE homology domain encompassing residues D156
191 and S157 (Supplementary Fig. 3F). Notably, S157 is altered in the MutB variant and corresponds
192 to tumor-associated mutations reported in COSMIC for MAGEA6 and the homologous MAGEA3.
193 Functional analysis showed that the D156E/S157Y double substitution weakened TRIM28 binding
194 and reduced MAGEA6-dependent ALKBH2 degradation (Fig. 3K, Supplementary Fig. 3H),
195 whereas the K211R substitution—located within the predicted ALKBH2-binding surface—had
196 only a modest effect on MAGEA6–ALKBH2 binding (Fig. 3J). Collectively, these results indicate
197 that D156 and S157 contribute to the MAGEA6–TRIM28 interface and suggest that this region
198 modulates MAGEA6-dependent regulation of ALKBH2, consistent with tumor-associated
199 variants disrupting the same site.

200

201 **MMS drives a biphasic ALKBH2 response, from acute degradation to prolonged**
202 **accumulation**

203 **MMS acutely promotes ALKBH2 degradation**

204 To investigate how MMS regulates the TRIM28–ALKBH2 axis, we analyzed their interaction
205 dynamics in H1299 cells. Short-term MMS exposure (3–6 h) increased the TRIM28–ALKBH2
206 association in a time- and dose-dependent manner (Fig. 4A, B). Both TRIM28 and ALKBH2 were

207 predominantly nuclear regardless of MMS treatment (Supplementary Fig. 4A). In contrast,
208 MAGEA3/6 accumulated in the nucleus upon MMS exposure (Fig. 4C), supporting the possibility
209 that MAGEA3/6 contributes to enhanced TRIM28–ALKBH2 assembly during genotoxic stress.
210 Consistent with this, MMS increased ALKBH2 K48-linked ubiquitination in a concentration-
211 dependent manner (Fig. 4D).

212 To exclude transcriptional effects, we used H1299 cells stably expressing TAP-tagged
213 ALKBH2 (Flag–HA tandem affinity tag). MMS accelerated ALKBH2 degradation, and this effect
214 was further enhanced by TRIM28 overexpression (Fig. 4E). Endogenous ALKBH2 similarly
215 showed reduced stability when cells were co-treated with MMS and cycloheximide (CHX),
216 compared with CHX alone (Supplementary Fig. 4B, C). These data support an early response
217 phase in which MMS promotes TRIM28-dependent ubiquitination and degradation of ALKBH2.

218 Because alkylating agents such as MMS and temozolomide (TMZ) elevate intracellular
219 ROS[58-60], we next examined whether redox conditions influence TRIM28–ALKBH2 binding. Co-
220 IP analysis showed that $H_2O_2$ increased complex formation, whereas ssDNA, ascorbate (Vc), or
221 EDTA reduced the interaction (Fig. 4F). Reduced glutathione (GSH) diminished TRIM28–
222 ALKBH2 binding, whereas oxidized glutathione (GSSG) had minimal effect; GSH also attenuated
223 the $H_2O_2$-induced increase (Supplementary Fig. 4D). EDTA similarly lowered basal interaction
224 and blocked $H_2O_2$-driven binding (Fig. 4G). In line with a redox-dependent mechanism, oxidative
225 stress alone promoted K48-linked polyubiquitination of ALKBH2 (Supplementary Fig. 4E).

226 The catalytically inactive ALKBH2(H171A/D173A) mutant[52,61] was refractory to both the
227 ssDNA-dependent reduction and the $H_2O_2$-induced enhancement of TRIM28 binding, indicating
228 that these redox-associated effects depend on ALKBH2 catalytic activity (Supplementary Fig. 4F).
229 The reducing agent Vc further suppressed MMS-induced K48-linked ubiquitination of ALKBH2
230 (Fig. 4H). Together, these results support an acute, redox-responsive phase in which TRIM28-
231 mediated ubiquitination drives ALKBH2 degradation.

232 **Prolonged MMS exposure stabilizes ALKBH2**

233 In contrast to the early degradative phase, prolonged MMS exposure (≥8 h) progressively
234 increased ALKBH2 protein levels in H1299 and H460 cells (Fig. 4I, J). By contrast, the related
235 demethylase ALKBH3 and MGMT showed no detectable change in protein levels. TRIM28
236 overexpression attenuated MMS-induced increase in ALKBH2 (Fig. 4K). These data indicate that
237 prolonged MMS exposure shifts ALKBH2 regulation from degradation toward stabilization.

238 **Prolonged MMS exposure induces transcriptional upregulation of ALKBH2**

239 To determine whether ALKBH2 accumulation involves transcriptional activation, we measured
240 ALKBH2 transcript levels in H1299 cells after MMS exposure for the indicated durations.
241 ALKBH2 mRNA increased at 12 h and remained elevated at 24 h (Fig. 4L), paralleling the delayed
242 protein induction.

243 Collectively, these data support a stress-dependent biphasic regulatory program, consisting of
244 an early TRIM28-dependent ubiquitination-and-degradation phase followed by a later phase
245 characterized by ALKBH2 stabilization together with transcriptional induction.

246

247 **MMS promotes K48-linked ubiquitination and proteasomal degradation of TRIM28,**
248 **coordinated by TRIM24 and MAGEA6**

249 To investigate how TRIM28 is regulated during alkylation stress, we examined its stability and
250 post-translational modification. MMS treatment caused a time- and dose-dependent reduction in
251 TRIM28 protein without altering its mRNA (Fig. 5A–C), and this loss was blocked by MG132,
252 indicating proteasome-mediated degradation. Prolonged low-dose MMS exposure (100 μM, 24–
253 72 h) led to a progressive increase in ALKBH2 protein levels, whereas ALKBH3, MGMT, and
254 MAGEA3/6 remained stable (Supplementary Fig. 5A). A 12-h MMS pre-exposure caused
255 TRIM28 depletion, increased basal ALKBH2, and a slower ALKBH2 degradation (Supplementary
256 Fig. 5B, C), consistent with reduced TRIM28 permitting ALKBH2 accumulation during sustained
257 alkylation stress.

258 To examine the mechanism underlying this regulation, we analyzed TRIM28 ubiquitination.
259 Denaturing IP of Flag-TRIM28 revealed that MMS strongly induced TRIM28 polyubiquitination

260 (Fig. 5D) and that this modification increased over time in H1299 cells (Fig. 5E). A K48-only
261 ubiquitin mutant confirmed that these conjugates are predominantly K48-linked and proteasome-
262 directed (Fig. 5F). K48-specific Halo-TUBE pulldown of endogenous TRIM28 further confirmed
263 MMS-induced ubiquitination under endogenous conditions (Fig. 5G). In contrast, other genotoxic
264 agents—including TMZ, CDDP, and $H_2O_2$—did not induce detectable K48-linked ubiquitination
265 or TRIM28 degradation (Fig. 5H, Supplementary Fig. 5D–F), indicating that TRIM28 loss is
266 selective for MMS-induced alkylation stress. The SUMO-acceptor-site TRIM28 mutant
267 (K554/779/804R)[62] showed markedly reduced K48-linked ubiquitination (Fig. 5I), indicating that
268 this lysine cluster is required for efficient MMS-induced modification.

269 To identify upstream factors influencing TRIM28 turnover, we analyzed the TRIM28
270 interactome (Supplementary Table 2) and validated selected interacting proteins. MMS increased
271 TRIM28 association with the E3 ligase TRIM24 and the proteasome subunits PSMD4 and PSMB5
272 in a time-dependent manner (Fig. 5J), and these interactions were weakened in the SUMO-acceptor
273 mutant (Supplementary Fig. 5G). MAGEA6 further enhanced assembly of the TRIM28–TRIM24
274 complex. Upon MMS exposure, MAGEA6 co-expression increased TRIM28 binding to TRIM24
275 and to PSMD4/PSMB5, accompanied by higher levels of K48-linked TRIM28 ubiquitination (Fig.
276 5K). Reciprocal co-IP using Flag-TRIM24 confirmed the MMS-inducible TRIM28–TRIM24
277 interaction and revealed that TRIM24 itself undergoes K48-linked ubiquitination (Fig. 5L).
278 Overexpression of TRIM24 amplified MMS-induced ubiquitination and promoted the reduction
279 of endogenous TRIM28 (Fig. 5M, Supplementary Fig. 5H, I). Collectively, these results indicate
280 that MMS induces K48-linked ubiquitination and proteasomal degradation of TRIM28 through a
281 pathway coordinated by MAGEA6, TRIM24, and SUMO-associated mechanisms, positioning
282 TRIM28 within an MMS-selective alkylation-responsive ubiquitin network.

283

284 **TRIM28–ALKBH2 axis connects patient outcome with alkylation-stress responses**

285 To assess the clinical relevance of this pathway in lung adenocarcinoma (LUAD), we examined
286 expression patterns of key alkylation repair enzymes. Analysis of TCGA transcriptomic and

287 CPTAC proteomic datasets showed increased ALKBH2 and decreased ALKBH3 in tumors
288 relative to normal lung tissue, whereas MGMT exhibited no significant change (Fig. 6A,
289 Supplementary Fig. 6A). Immunohistochemistry further confirmed stronger ALKBH2 staining in
290 LUAD than in matched normal samples (Fig. 6B). A similar expression pattern was observed in
291 NSCLC cell lines, which showed higher ALKBH2 and lower ALKBH3 compared with BEAS-2B
292 bronchial epithelial cells (Fig. 6C). In survival analyses, elevated ALKBH2 correlated with poorer
293 overall survival, whereas higher ALKBH3 associated with improved prognosis (Fig. 6D, E).

294 Because cigarette smoking generates alkylating and methylating DNA lesions[63], we next
295 analyzed ALKBH2 expression according to smoking status. ALKBH2 transcripts were higher in
296 LUAD patients with a smoking history than in non-smokers (Supplementary Fig. 6B). Somatic
297 mutations in MAGEA6, a component of the TRIM28–ALKBH2 pathway, were also more frequent
298 in smokers, whereas MAGEA3 mutations showed no enrichment (Supplementary Fig. 6C). These
299 observations suggest an association between ALKBH2 and smoking-linked alkylation stress and
300 implicate MAGEA6 in regulatory control of this pathway.

301 To relate these clinical patterns to cellular stress responses, we employed an acute MMS-
302 exposure model. Because prolonged MMS treatment reduces TRIM28 and induces delayed
303 ALKBH2 accumulation, we applied a brief high-dose MMS pulse (500 μM, 1 h) that induced γ-
304 H2AX with minimal effects on TRIM28 and ALKBH2 protein levels (Supplementary Fig. 6D).
305 Under these conditions, ALKBH2 knockdown using two independent shRNAs reduced cell
306 viability and markedly increased MMS sensitivity (Fig. 6F, G). TRIM28 overexpression did not
307 alter basal proliferation (Supplementary Fig. 6E) but enhanced MMS sensitivity in a RING-
308 dependent manner, and this phenotype was restored by re-expression of wild-type TRIM28 in
309 knockdown cells (Fig. 6H, I). Co-expression of ALKBH2 reversed the sensitization, supporting a
310 model in which ALKBH2 acts downstream of TRIM28 during acute alkylation stress (Fig. 6J).
311 These data indicate that ALKBH2 acts downstream of TRIM28 in the acute MMS response.

312 We next examined whether MAGEA6 modulates this regulatory arm. MAGEA6
313 overexpression increased MMS sensitivity, whereas its knockdown conferred resistance; re-

314 expression restored sensitivity (Supplementary Fig. 6F). MAGEA6 failed to enhance MMS
315 cytotoxicity when TRIM28 was depleted, and a TRIM28-binding-deficient mutant (D156E/S157Y)
316 showed markedly reduced activity (Fig. 6K, L). In contrast, MAGEA6 did not affect responses to
317 cisplatin (CDDP) or the proteasome inhibitor bortezomib (Supplementary Fig. 6G, H), indicating
318 that its regulatory effect is specific to alkylation stress rather than general cytotoxic stress.
319 Collectively, these data suggest that the TRIM28–ALKBH2 pathway, reinforced by MAGEA6,
320 contributes to cellular tolerance to alkylation damage and is consistent with differences observed
321 in chemotherapy-associated patient outcomes.
322
323 **TRIM28–ALKBH2 axis couples MMS sensitization with cisplatin response in NSCLC**
324 Prior studies indicate that the TRIM28/*miR*-125b-5p/CREB1 axis enhances CDDP resistance in
325 NSCLC[64]. To evaluate the clinical relevance of TRIM28, we analyzed 771 NSCLC cases. Among
326 patients who received systemic therapy, platinum-based regimens—mainly CDDP-containing
327 combinations—were the predominant treatment modality (Supplementary Fig. 7A). High TRIM28
328 expression was associated with poorer overall survival in chemotherapy-treated patients, whereas
329 no prognostic association was observed in patients who did not receive chemotherapy
330 (Supplementary Fig. 7B, C). These data indicate that TRIM28 expression is linked to adverse
331 prognosis specifically in the setting of cytotoxic chemotherapy, consistent with a putative role in
332 promoting platinum resistance.
333 To investigate how TRIM28 influences cellular responses beyond cisplatin treatment, we
334 established a chronic MMS exposure model. MMS $IC_{50}$ values were determined in NSCLC cells.
335 The MMS $IC_{50}$ values were approximately 141.5 μM in H1299 cells and 236.8 μM in H460 cells
336 (Supplementary Fig. 7D). For dose–response assays, we used concentrations around the $IC_{50}$ range;
337 H1299 cells were exposed to 40–120 μM MMS for 48 h. TRIM28 depletion increased MMS
338 resistance in these cells (Fig. 7A). For long-term clonogenic assays, H460 cells, which form robust
339 colonies, were treated with 100 μM MMS for 48 h and then allowed to recover for 7 days in drug-
340 free medium. TRIM28 overexpression in H460 cells increased MMS sensitivity and reduced

341 colony formation (Fig. 7B, C). TRIM28 increased cellular sensitivity to sustained MMS-induced
342 alkylation stress, a pattern distinct from its association with poor prognosis under platinum-based
343 chemotherapy.

344 Given the opposite effects of TRIM28 on MMS sensitization and cisplatin response, we first
345 examined how TRIM28 influences cellular responses under MMS–CDDP co-treatment. Because
346 2 μM CDDP induces only limited cytotoxicity, we used this dose as a low-background condition
347 to assess combinatorial effects. TRIM28 overexpression increased MMS sensitivity, and co-
348 treatment with MMS and CDDP further reduced cell viability, indicating that CDDP exposure
349 amplifies TRIM28-mediated MMS sensitization (Fig. 7D). To determine whether ALKBH2
350 accounts for this effect, we evaluated MMS and CDDP responses in ALKBH2-depleted cells.
351 Since MMS induces ALKBH2 expression, we used H1299 cells with stable ALKBH2 knockdown
352 to avoid confounding from induction. Re-expression of ALKBH2 substantially restored MMS
353 tolerance, consistent with its role in repairing alkylation damage. However, when combined with
354 MMS, 2 μM CDDP markedly weakened ALKBH2-mediated protection, leading to a pronounced
355 increase in MMS-induced cell death (Fig. 7E). These observations suggest that TRIM28-driven
356 MMS sensitization is attributable to its suppression of ALKBH2, and that the protective effect of
357 ALKBH2 is diminished under MMS–CDDP co-treatment.

358 To investigate why CDDP diminishes ALKBH2-mediated protection, we examined whether
359 oxidative stress–associated DNA damage contributes to this sensitization. Because CDDP can
360 induce reactive oxygen species (ROS), including $H_2O_2$[65], we tested whether oxidative stress
361 potentiates MMS-induced cytotoxicity. Co-treatment of MMS with increasing concentrations of
362 $H_2O_2$ reduced cell viability in a dose-dependent manner (Supplementary Fig. 7E), consistent with
363 the enhanced cytotoxicity observed under MMS–CDDP co-treatment. To corroborate these effects
364 on DNA integrity, alkaline comet assays showed that low doses of CDDP (2 μM) or MMS (50
365 μM) alone induced limited DNA strand breaks, whereas co-treatment substantially increased tail
366 moments (Fig. 7E) and γ-H2AX accumulation (Supplementary Fig. 7F). These observations

367 indicate that oxidative and alkylating stresses cooperate to enhance DNA damage during MMS–
368 CDDP co-treatment.

369 To determine the functional consequences of this interaction, we next evaluated whether low-
370 level alkylation stress modulates cisplatin sensitivity. Sub-$IC_{50}$ MMS decreased the $IC_{50}$ of CDDP
371 in both H1299 and H460 cells (Fig. 7F, G), consistent with enhanced cisplatin sensitivity under
372 mild alkylation stress. To assess long-term cellular responses, we performed colony formation
373 assays, in which MMS–CDDP co-treatment further reduced clonogenic survival (Fig. 7H, I). In
374 three-dimensional tumor spheroids, the combination similarly reduced spheroid size and viability
375 (Fig. 7J, K). Collectively, these results indicate that the TRIM28–ALKBH2 axis contributes to
376 MMS sensitization, and that CDDP further amplifies this effect under combined MMS–CDDP
377 exposure by weakening ALKBH2-mediated protection during co-treatment.

## DISCUSSION

Building on our previous work identifying the deubiquitinase OTUD4 as a regulator of an AlkB-family demethylase[2], this study identifies the TRIM28–MAGEA6 ubiquitin pathway that regulates ALKBH2 stability. Proteomic profiling of the alkylation-responsive ASCC complex—functionally linked to ALKBH3 and detected together with ALKBH2[35]—identified TRIM28 as an ASCC2-associated component, suggesting that TRIM28 links transcription-associated assemblies to ubiquitin-dependent regulation during alkylation repair. In this study, we identify TRIM28, together with the cancer-testis antigen MAGEA6, as the E3 ligase complex that controls ALKBH2 stability through K48-linked ubiquitination and proteasomal degradation (Fig. 1–3). Under basal conditions, the TRIM28–MAGEA6 complex limits ALKBH2 protein level, whereas ALKBH2 increases TRIM28 transcription, forming a reciprocal feedback loop that maintains steady-state repair capacity. Alkylation stress reorganizes this loop in a time-dependent manner: during acute MMS exposure, increased TRIM28–ALKBH2 association promotes ALKBH2 ubiquitination and degradation, whereas prolonged exposure shifts ubiquitin flux toward TRIM28, which coincides with its degradation and the subsequent stabilization and transcriptional induction of ALKBH2 (Fig. 8).

This study identifies TRIM28, together with the cancer-testis antigen MAGEA6, as the E3 ligase complex that controls ALKBH2 stability through K48-linked ubiquitination, providing the first ubiquitin-dependent mechanism for regulating ALKBH2 protein level. This regulatory module reveals how substrate binding, DNA accessibility, and transcription-linked feedback converge to regulate ALKBH2. Although the AlkB family participates in multiple steps of nucleic acid repair[66], the post-translational mechanisms governing individual family members remain incompletely defined. Distinct E3 ligases have been linked to other AlkB homologues, including TRIM28 for ALKBH5[19] and TRIM21 for FTO[18]. In contrast to these RNA-modifying enzymes, ALKBH2 repairs methylated bases within duplex DNA, and the ubiquitin-dependent mechanisms regulating its stability—including both E3- and DUB-linked control—remained uncharacterized. Unlike canonical MAGE–TRIM architectures[67,68], MAGEA6 binds both TRIM28 and ALKBH2

405 (Fig. 3B), indicating a dual-binding mode that contributes to their association under alkylation
406 stress. Although ALKBH2 and ALKBH3 share conserved catalytic cores, TRIM28 preferentially
407 interacts with ALKBH2 (Fig. 1I), a selectivity attributable to the ALKBH2-specific finger motif
408 and long-loop region required for DNA binding[52]. Docking analysis predicts that the TRIM28-
409 contacting surface lies adjacent to the DNA-binding region of ALKBH2 (Fig. 1J), and ssDNA
410 competitively reduces their association (Fig. 1K). These observations are consistent with a model
411 in which DNA occupancy transiently limits TRIM28 binding to ALKBH2, allowing catalytic
412 turnover to proceed and enabling ubiquitin-dependent regulation once ALKBH2 dissociates from
413 damaged DNA. Under basal conditions, ALKBH2 increased TRIM28 mRNA and protein levels
414 (Fig. 2J–L), forming the transcriptional arm of this reciprocal loop, consistent with evidence that
415 ALKBH2 modulates promoter methylation and the transcription of targets such as MGMT and
416 BMI1[69,70]. Together with evidence that the deubiquitinase OTUD4 associates with ALKBH2 and
417 ALKBH3[2], these results suggest that AlkB-family enzymes operate within a broader ubiquitin-
418 regulated framework, in which the TRIM28–MAGEA6 module contributes to maintaining
419 demethylase homeostasis under basal and stress conditions.

420 TRIM28 is itself regulated under alkylation stress, adding a second layer of control within the
421 TRIM28–ALKBH2 pathway. MMS uniquely induced K48-linked polyubiquitination and
422 proteasomal degradation of TRIM28 (Fig. 5A–G), whereas other genotoxic agents—including
423 temozolomide (TMZ), cisplatin (CDDP), and $H_2O_2$—did not cause detectable TRIM28
424 modification or loss (Fig. 5H, Supplementary Fig. 5D–F). These agents instead produced TRIM28-
425 independent changes in ALKBH2: TMZ increased ALKBH2 protein levels without reducing
426 TRIM28, $H_2O_2$ decreased ALKBH2, and CDDP produced minimal change. The TMZ-driven
427 increase in ALKBH2 is consistent with previous studies showing transcriptional induction in
428 glioblastoma cells[11], indicating that TMZ predominantly affects transcriptional rather than post-
429 translational regulation. MMS-induced ubiquitination of TRIM28 was markedly reduced in the
430 SUMO-site mutant K554/779/804R (Fig. 5I), implying that this lysine cluster either contributes to
431 ubiquitin acceptance or modulates ubiquitination efficiency. In parallel, TRIM24 association

432 further increased TRIM28 ubiquitination under MMS exposure (Fig. 5K–L), indicating that
433 TRIM24 cooperates with MMS-responsive ubiquitin signaling to promote TRIM28 degradation.
434 This stress-linked regulation is mechanistically distinct from the RNF4-dependent degradation of
435 phosphorylated and SUMOylated TRIM28 described during double-strand break repair[48],
436 suggesting that distinct DNA lesions are likely coupled to separate ubiquitin pathways. Additional
437 MMS-dependent regulatory features reinforce the specificity of this pathway. MMS promotes
438 HLTF degradation without affecting UV-induced PCNA monoubiquitination[71] and activates
439 RNF113A to recruit the ASCC–ALKBH3 complex[72]. These observations place TRIM28 within
440 an alkylation-selective ubiquitin framework, in which MMS engages a ubiquitin-mediated
441 turnover route linked to repair adaptation. Notably, TRIM24 and TRIM28 are known to cooperate
442 in transcriptional programs across multiple cancer settings, where TRIM28 stabilizes TRIM24 and
443 enhances its transcriptional output[73,74]. Under MMS exposure, however, TRIM24 promoted
444 TRIM28 ubiquitination and accelerated its degradation (Fig. 5J, M, Supplementary Fig. 5H–I),
445 indicating a stress-dependent reversal of this regulatory relationship. This MMS-specific
446 mechanism decreases TRIM28 stability and may support remodeling of chromatin-associated
447 repair assemblies during persistent alkylation stress.

448 A key mechanistic insight from this study is the identification of a time-dependent TRIM28–
449 ALKBH2 feedback loop that modulates DNA repair capacity during alkylation stress. This loop
450 functions as a biphasic regulatory switch, sequentially balancing repression and activation phases.
451 During acute MMS exposure, TRIM28 binds to ALKBH2 and promotes its K48-linked
452 ubiquitination and proteasomal degradation, thereby transiently limiting repair activity (Fig. 4).
453 As MMS exposure persists, TRIM28 becomes ubiquitinated and degraded, whereas ALKBH2 is
454 stabilized and transcriptionally induced (Fig. 4–5), marking a temporal transition from suppression
455 toward activation of repair function. This temporal shift parallels the behavior of demethylation
456 repair, in which ALKBH2 catalyzes oxidative removal of methylated bases after binding to DNA
457 lesions. The biphasic pattern is consistent with broader principles of stress adaptation, paralleling
458 the time-delayed feedback observed in the ATM–KAP1 (TRIM28) and p53–MDM2 circuits that

459 coordinate DNA repair signaling with checkpoint recovery[75,76]. Unlike these canonical pathways,
460 the TRIM28–ALKBH2 module integrates both ubiquitin- and transcription-linked feedback,
461 enabling the E3 ligase and its substrate to function as reciprocal regulators. Under basal conditions,
462 ALKBH2 increases TRIM28 expression at both mRNA and protein levels (Fig. 2J–L), maintaining
463 repair homeostasis. Under prolonged alkylation stress, TRIM28 depletion, together with ALKBH2
464 stabilization and transcriptional induction, shifts the system toward higher ALKBH2 levels and
465 more efficient handling of sustained damage. This time-dependent response likely enables cells to
466 adjust repair activity in response to both the duration and intensity of exposure, thereby modulating
467 the repair environment during chemotherapy.

468 Clinically, ALKBH2 is frequently elevated in lung adenocarcinoma and is associated with
469 poorer overall survival (Fig. 6A–D), consistent with its capacity to counteract alkylation
470 damage[12,25]. In contrast, TRIM28 is associated with overall survival only in chemotherapy-treated
471 patients, where higher expression is associated with shorter survival (Supplementary Fig. 7A–C),
472 indicating that its clinical impact emerges under treatment-induced stress rather than at baseline.
473 Somatic MAGEA6 alterations, which are enriched among smokers (Supplementary Fig. 6C), may
474 further modulate this circuit by regulating the activity of the TRIM28–MAGEA6 ubiquitin module.
475 Given that tobacco exposure increases endogenous alkylation load[77], functional variation in
476 MAGEA6 is likely to shape pathway behavior under sustained damage, thereby contributing to
477 interpatient differences in repair capacity and chemotherapy sensitivity.

478 Functionally, TRIM28 enhances MMS cytotoxicity by promoting ALKBH2 loss, whereas
479 ALKBH2 re-expression reverses this effect (Fig. 6F–I), indicating that ALKBH2 is the dominant
480 mediator of TRIM28-linked sensitivity. Combining MMS with CDDP increased DNA damage,
481 reduced clonogenic survival, and counteracted ALKBH2-dependent alkylation tolerance (Fig. 7B–
482 K). In ALKBH2-high cells, CDDP almost completely abolished the protection conferred by
483 ALKBH2, reducing MMS tolerance to the level observed in ALKBH2-knockdown cells (Fig. 7E).
484 Although TRIM28 has been linked to NSCLC chemoresistance through pathways involving *miR*-
485 125b-5p/CREB1 signaling, E2F1 regulation, or DNA-damage control[64,78-81], TRIM28 acts

upstream to promote ALKBH2 degradation in this MMS-based system. This context dependence is consistent with the distinct DNA lesions and stress signals generated by alkylating agents versus platinum crosslinkers, and suggests that the nature and duration of genotoxic stress modulate TRIM28 activity. Together, these observations support a model (Fig. 8) in which the time-dependent TRIM28–ALKBH2 loop integrates alkylation stress, ubiquitin signaling, and ALKBH2 availability to influence treatment response, suggesting that platinum-containing regimens may be more effective when TRIM28 is destabilized or ALKBH2 supply becomes limiting.

In summary, this study identifies a stress-dependent TRIM28–ALKBH2 feedback loop that modulates alkylation repair capacity in NSCLC cells. Under basal conditions, the TRIM28–MAGEA6 complex mediates K48-linked polyubiquitination and proteasomal turnover of ALKBH2. Acute MMS exposure enhances assembly of the TRIM28–ALKBH2 complex and promotes ALKBH2 degradation, whereas prolonged MMS exposure induces K48-linked ubiquitination and proteasomal degradation of TRIM28, leading to ALKBH2 stabilization and transcriptional upregulation. This stress-responsive loop links post-translational regulation with transcription-associated control of ALKBH2, collectively shaping cellular responses to alkylating agents. The upstream cues that trigger TRIM28 degradation and how these signals interface with transcriptional programs remain to be defined. Future studies in patient-derived and *in vivo* models will help clarify these regulatory steps and assess their relevance to chemotherapy response in NSCLC.

505 **Methods**

506 **Cell culture**

507 HEK293T cells (ATCC CRL-11268, USA) and the non–small cell lung cancer (NSCLC) cell lines
508 H1299 (SCSP-589, Cell Bank of the Chinese Academy of Sciences, China), A549 (SCSP-503,
509 Cell Bank of the Chinese Academy of Sciences, China), and NCI-H460 (SCSP-584, Cell Bank of
510 the Chinese Academy of Sciences, China) were maintained in Dulbecco's modified Eagle's
511 medium (DMEM; C11995500BT, Gibco, USA) supplemented with 10% heat-inactivated fetal
512 bovine serum (FBS; 10099-141C, Gibco, USA) and penicillin–streptomycin. Cells were cultured
513 at 37 °C in a humidified 5% $CO_2$ incubator, and all experiments were performed using low-passage
514 cells (passages 5–15). All cell lines were routinely confirmed to be mycoplasma-free using a
515 luminescence-based detection assay (C0297, Beyotime, China).

516

517 **Plasmid constructs, mutagenesis, and viral infection**

518 Full-length human TRIM28 and ALKBH2 cDNAs were used as templates for PCR-based site-
519 directed mutagenesis. TRIM28 deletion and point mutants, including the BCC fragment (residues
520 141–400) and the RING-inactive C65/68A mutant, were generated by PCR, cloned into pENTR-
521 4, and transferred into pHAGE-CMV-Flag/HA/His through Gateway™ LR recombination
522 (11791020, Invitrogen, USA). ALKBH2 variants were cloned into pCMV-Flag for mammalian
523 expression and into pET28a-His-2×Flag for bacterial expression. All constructs were verified by
524 Sanger sequencing. Wild-type MAGEA6 cDNA was generated by reverse transcription of A549
525 RNA, and H1299-derived MAGEA6 variants were generated analogously. Transient transfections
526 were performed using Lipo8000 (C0533, Beyotime, China).

527 Lentiviruses were produced in HEK293T cells by co-transfecting pLKO.1 or pHAGE vectors
528 with the packaging plasmids psPAX2 and pMD2.G. Viral supernatants were collected 48–72 h
529 post-transfection, clarified, and passed through 0.45-μm filters. Target cells were infected in the
530 presence of polybrene (6 μg/mL) for 12 h. Stable cell lines were selected with puromycin (1 μg/mL)

531 or blasticidin (5 μg/mL) for 3 days and maintained under selection-free conditions unless
532 otherwise indicated.
533
534 **Immunoprecipitation and western blotting**
535 For overexpression immunoprecipitation (IP), HEK293T cells were transfected with the indicated
536 plasmids using Lipo8000 and cultured for 48–72 h before lysis. Cells were lysed in a buffer
537 containing 150 mM NaCl, 50 mM Tris-HCl (pH 7.9), 1% Triton X-100, 10% glycerol, and 2 mM
538 DTT, supplemented with protease and phosphatase inhibitors. Clarified lysates were incubated
539 overnight at 4 °C with anti-Flag M2-agarose beads (A2220, Sigma-Aldrich, USA) or anti-HA-
540 agarose beads (B26201, Selleck, China). For denaturing IP, lysates were boiled in TBS containing
541 1% SDS and then diluted with lysis buffer to a final SDS concentration of 0.1% before IP. Each
542 co-IP experiment was performed at least twice independently, and IP samples were analyzed by
543 WB two to three times with consistent results.
544 For endogenous IP in H1299 cells, lysates were prepared using the same buffer and cleared
545 by centrifugation (15,000 × *g*, 10 min, 4 °C). Supernatants were pre-cleared with Protein A/G
546 magnetic beads (B23202, Selleck, China) for 1 h and incubated overnight at 4 °C with anti-
547 TRIM28 (1.5 μg). Immune complexes were captured with Protein A/G magnetic beads, washed
548 with lysis buffer, and eluted in Laemmli sample buffer. Input and flow-through fractions were
549 analyzed in parallel by western blotting (WB) to verify expression and loading.
550 For ssDNA competition assays, purified Flag-ALKBH2 was added to HEK293T whole-cell
551 lysates supplemented with synthesized single-stranded DNA (ssDNA) oligonucleotides and
552 incubated overnight at 4 °C. Disruption of the TRIM28–ALKBH2 interaction was assessed by
553 Flag IP followed by WB.
554 For WB, proteins were separated by SDS–PAGE and transferred to PVDF membranes.
555 Membranes were blocked with 5% non-fat milk in TBST for 1 h at room temperature, incubated
556 with primary antibodies overnight at 4 °C, and then with HRP-conjugated secondary antibodies

557 for 1–1.5 h at room temperature. Signals were detected using enhanced chemiluminescence (ECL).
558 Information on antibodies used in this study is provided in Supplementary Table 5.
559
560 **shRNA and CRISPR/Cas9 knockdown/knockout**
561 For shRNA-mediated knockdown, annealed oligonucleotides encoding target-specific sequences
562 were cloned into the pLKO.1 vector (8453, Addgene, USA) and packaged into lentiviral particles
563 using HEK293T cells. Target cells were transduced and selected with puromycin for 3 days to
564 establish stable knockdown lines. Knockdown efficiency was confirmed by WB. A non-targeting
565 shRNA was used as a control.
566 For CRISPR/Cas9-mediated knockout of TRIM28, single-guide RNAs (sgRNAs) were
567 designed according to established criteria and cloned into the lentiCRISPRv2 vector (52961,
568 Addgene, USA). Lentiviral particles were produced in HEK293T cells and used to transduce target
569 cells, followed by puromycin selection. Single-cell clones were isolated by limiting dilution and
570 expanded in 96-well plates, and successful knockout was verified by WB. All oligonucleotide
571 sequences are listed in Supplementary Table 3.
572
573 ***In vitro* MBP pull-down assay**
574 Recombinant MBP-tagged TRIM28 (MBP–TRIM28), MBP–MAGEA6, His-Flag-tagged
575 ALKBH2 (His-Flag–ALKBH2), and MBP alone were expressed in *E. coli* Rosetta (DE3). Protein
576 expression was induced with IPTG, and bacterial pellets were collected, lysed, and purified on
577 amylose resin.
578 For pull-down assays, purified MBP-TRIM28, MBP-MAGEA6, or MBP alone was
579 immobilized on amylose resin (E8021S, NEB, USA) and washed with binding buffer. The resin
580 was incubated with purified His-Flag–ALKBH2 at 4 °C with gentle mixing. After thorough
581 washing, bound proteins were eluted in Laemmli sample buffer at 95 °C and analyzed by WB
582 using anti-His or anti-Flag antibodies.
583

584 **Immunofluorescence (IF)**

585 Cells grown on glass coverslips were treated as indicated, fixed in 4% paraformaldehyde (P0099,
586 Beyotime, China) for 30 min, and permeabilized with 0.5% Triton X-100 in PBS for 15 min at
587 room temperature. After washing in PBST, samples were incubated with primary antibodies
588 overnight at 4 °C. The next day, coverslips were washed and incubated with fluorophore-
589 conjugated secondary antibodies together with Hoechst 33342 or DAPI for 1.5 h at room
590 temperature. Coverslips were mounted and imaged using an Olympus fluorescence microscope.
591 Colocalization analysis was performed in ImageJ, and Pearson correlation coefficients were
592 calculated when applicable.

593

594 **Cycloheximide chase assay**

595 For cycloheximide (CHX) (2112, CST, USA) chase assays, cells were treated with 150 μg/mL
596 CHX for the indicated durations. Cells were harvested at each time point and analyzed by WB to
597 evaluate protein stability.

598

599 **RNA isolation and qRT-PCR**

600 Total RNA was isolated using the RNAeasy™ RNA Isolation Kit (R0026, Beyotime, China). RNA
601 concentration and purity were assessed using a NanoDrop spectrophotometer (Thermo Fisher
602 Scientific) by measuring absorbance at 260 nm and determining the A260/A280 and A260/A230
603 ratios. First-strand cDNA was synthesized using the PrimeScript™ RT reagent Kit (RR047A,
604 Takara, Japan), and qPCR was performed using the SYBR Green qPCR Mix (TSE501, Tsingke,
605 China). Gene expression was normalized to β-actin. Primer sequences are listed in Supplementary
606 Table 4.

607 **Protein–protein docking and structural modeling**

608 The tertiary structures of human ALKBH2 (PDB ID: 3BTZ), ALKBH3 (PDB ID: 2NCU), and the
609 RBCC domain of TRIM28 (PDB ID: 6QAJ) were retrieved from the Protein Data Bank
610 (http://www.rcsb.org). Protein–protein docking simulations were performed using the GRAMM-

611 X web server (http://gramm.compbio.ku.edu). Predicted interfaces between TRIM28 and
612 MAGEA6 were generated using AlphaFold3 (https://alphafoldserver.com/). Docking models were
613 visualized and inspected using PyMOL (Version 2.6.0a0).

614 **Mass spectrometry**

615 TRIM28 complexes from H1299 cells stably expressing TAP-TRIM28 were immunoaffinity-
616 purified using anti-Flag M2-agarose beads and eluted with Flag peptide (F3290, Sigma, USA).
617 Eluates were separated by SDS–PAGE, visualized by silver staining, and subjected to LC–MS/MS.
618 Mass spectrometry analysis was performed on an Easy nLC 1200 system (Thermo Fisher
619 Scientific) coupled to a Dr. Maisch GmbH C18 column (75 μm × 150 mm, 3 μm). Data-dependent
620 acquisition (DDA) was carried out on a Q-Exactive HF-X mass spectrometer (Thermo Fisher
621 Scientific). Peptide spectra were searched against the UniProt Homo sapiens Reference Proteome
622 (UP000005640; 81791-20230317.fasta).

623

624 **Affinity purification of K48-linked polyubiquitinated proteins (Halo-TUBE)**

625 K48-linked polyubiquitin chains and polyubiquitinated proteins were affinity-purified under
626 denaturing conditions using Halo-tagged tandem ubiquitin-binding entity (Halo-TUBE) resin.
627 Briefly, cells were harvested, lysed, and denatured by boiling in TBS containing 1% SDS, then
628 diluted with lysis buffer to reduce SDS to 0.1% before affinity purification. Extracts were
629 incubated with HaloLink resin (G1915, Promega, USA) pre-bound to purified Halo-TUBE protein
630 (10 μg per sample) overnight at 4 °C with rotation. The resin was washed five times with washing
631 buffer, and bound proteins were eluted by boiling in Laemmli sample buffer and analyzed by WB.

632

633 **Cell proliferation, CDDP sensitivity, and synergy assays**

634 For the methyl methanesulfonate (MMS; 129925, Sigma, USA) sensitivity assay, cells (2,000–
635 5,000 per well, in 96-well plates) were exposed to high-dose MMS (200–800 μM) for 1 h at 37 °C,
636 followed by replacement with fresh medium, or were continuously treated with low-dose MMS

637 (0–200 μM) for 48 h. Cell viability was measured at 48 h using the CCK-8 assay (K1018, ApexBio,
638 USA).
639 For the cisplatin (CDDP) sensitivity assay, cells were treated with CDDP (0–40 μM) (HY-
640 17394, MCE, USA) for 48 h, and viability was assessed using the CCK-8 assay. $IC_{50}$ values were
641 calculated using GraphPad Prism.
642 For the synergy assay, cells were treated with CDDP alone or together with low-dose MMS
643 for 48 h, and viability was quantified using CCK-8.
644

645 **Colony formation assay**

646 For clonogenic assays, H460 cells were seeded in 24-well plates (400 cells per well) and allowed
647 to adhere overnight. The following day, cells were treated with DMSO (vehicle) or with MMS at
648 the indicated concentrations. For combination treatment, the medium was replaced after 48 h of
649 MMS alone, CDDP alone, or MMS–CDDP co-treatment. Cells were then cultured for 5–10 days
650 to allow colony formation, fixed in 4% paraformaldehyde for 10 min, stained with 0.1% crystal
651 violet (C0121, Beyotime, China), washed, air-dried, and counted.

652 **Alkaline comet assay**

653 Alkaline single-cell gel electrophoresis (comet) assays were performed using a Comet Assay Kit
654 (KGA1302, Keygentec, China) according to the manufacturer's instructions. Comet images were
655 captured using an Olympus fluorescence microscope. Tail DNA% and Tail Moment were
656 quantified in ImageJ (Version 1.54K) using the Comet Assay plugin. Tail DNA% was calculated
657 as: Tail DNA% = (Tail DNA Intensity / (Tail DNA Intensity + Head DNA Intensity)) × 100%;
658 Tail Moment was calculated as: Tail Moment = Tail Length × Tail DNA%.

659 **3D tumorsphere culture**

660 H1299 cells (~2,000 cells per drop) were cultured as hanging drops for 72 h to allow spheroid
661 formation, then transferred to ultra-low-attachment 96-well plates (LV-ULA002-96UW, Liver
662 Biotech, China). Tumor spheroids were treated with MMS and/or CDDP at the indicated

663 concentrations for 48 h. After treatment, the medium was replaced with fresh culture medium, and
664 spheroids were maintained for 3–4 weeks. Viability and cytotoxicity were assessed using a
665 Calcein-AM/Propidium Iodide (PI) Live/Dead assay kit (C2015S, Beyotime, China). Live (green)
666 and dead (red) fluorescence was imaged using an Olympus fluorescence microscope.

667 **Bioinformatics and clinical data analysis**

668 Clinical information for TCGA LUAD and LUSC patients was obtained from the TCGA data
669 portal (https://portal.gdc.cancer.gov/). Gene-expression profiles from TCGA and protein-
670 expression data from CPTAC were analyzed using UALCAN (http://ualcan.path.uab.edu/).
671 Survival analyses were performed using the Kaplan–Meier Plotter (http://kmplot.com/analysis)
672 under default settings, and hazard ratios and log-rank p-values were reported. ALKBH2
673 immunohistochemistry (IHC) images were obtained from the Human Protein Atlas
674 (http://www.proteinatlas.org). MAGEA6 and MAGEA3 mutation data were examined using
675 COSMIC (http://cancer.sanger.ac.uk/cosmic) and cBioPortal (http://www.cbioportal.org). Cutoffs
676 and covariates used in each analysis are provided in the corresponding figure legends.

677 **Statistics and reproducibility**

678 All statistical analyses were performed using GraphPad Prism (version 9.5.0). Data are presented
679 as mean ± standard deviation (s.d.). Key functional assays (viability, $IC_{50}$ measurements, and
680 ubiquitination assays) were repeated in at least three independent experiments, as specified in the
681 figure legends. Assays with intrinsically high within-experiment sampling—including co-IP,
682 Halo-TUBE, WB, IF, and qRT–PCR—were repeated in at least two independent experiments,
683 each incorporating multiple biological or technical replicates. Colony formation, comet assays,
684 and 3D tumorsphere assays were performed in two independent experiments, each with large per-
685 experiment sample sizes (colonies, cells, or spheroids), as specified in the figure legends. Two-
686 group comparisons were performed using two-tailed unpaired Student's t-tests unless otherwise
687 specified, and Mann–Whitney tests were applied to non-parametric datasets. Log-rank tests were
688 used for survival analyses, and Pearson correlation coefficients (PCCs) were calculated for

689 colocalization. $IC_{50}$ values were obtained from four-parameter logistic fitting. P-values for
690 MAGEA3/6 mutation frequencies were calculated using Fisher's exact test. All statistical tests and
691 sample sizes are reported in the figure legends.
692
693 **Reporting summary**
694 Further information on research design is available in the Nature Portfolio Reporting Summary
695 linked to this article.
696
697 **Data availability**
698 The data supporting the findings of this study are available within the paper and its Supplementary
699 Information.
700
701 **Acknowledgments**
702 This work was supported by the National Natural Science Foundation of China (Grant No.
703 31971232) and the Natural Science Foundation of Hunan Province (Grant No. 2019JJ40185) to
704 YZ.
705
706 **Author contributions**
707 **Zhiming Sun**: Writing – original draft, Visualization, Resources, Investigation, Data curation.
708 **Yunfang Deng**: Formal analysis, Investigation, Data curation. **Yue Liu**: Investigation. **Zhaohui**
709 **Liu**: Visualization, Formal analysis. **Jiabing Li**: Visualization, Formal analysis. **Lihui Wu**:
710 Investigation. **Liyuan Zeng**, **Xiaorong Feng**, **Lin Miao**: Investigation, Data curation. **Ying Sheng**,
711 **Bei Chen**, **Yuming He**, **Ye Liu**: Investigation. **Yu Zhao**: Writing – review & editing, Visualization,
712 Supervision, Funding acquisition, Conceptualization.
713
714 **Competing interests**
715 The authors declare no competing interests.

716 **References**


717 1 Fu, D., Calvo, J. A. & Samson, L. D. Balancing repair and tolerance of DNA damage caused by alkylating
718 agents. *Nat Rev Cancer* **12**, 104-120, doi:10.1038/nrc3185 (2012).
719 2 Zhao, Y. *et al.* Noncanonical regulation of alkylation damage resistance by the OTUD4 deubiquitinase. *The*
720 *EMBO journal* **34**, 1687-1703, doi:10.15252/embj.201490497 (2015).
721 3 Soll, J. M., Sobol, R. W. & Mosammaparast, N. Regulation of DNA Alkylation Damage Repair: Lessons and
722 Therapeutic Opportunities. *Trends in biochemical sciences* **42**, 206-218, doi:10.1016/j.tibs.2016.10.001
723 (2017).
724 4 Li, J. *et al.* USP7 promotes temozolomide resistance by stabilizing MGMT in glioblastoma. *Cell death &*
725 *disease* **16**, 631, doi:10.1038/s41419-025-07969-3 (2025).
726 5 Chen, X. *et al.* A novel enhancer regulates MGMT expression and promotes temozolomide resistance in
727 glioblastoma. *Nature communications* **9**, 2949, doi:10.1038/s41467-018-05373-4 (2018).
728 6 Trewick, S. C., Henshaw, T. F., Hausinger, R. P., Lindahl, T. & Sedgwick, B. Oxidative demethylation by
729 Escherichia coli AlkB directly reverts DNA base damage. *Nature* **419**, 174-178, doi:10.1038/nature00908
730 (2002).
731 7 Leiros, I. *et al.* Structural basis for enzymatic excision of N1-methyladenine and N3-methylcytosine from
732 DNA. *The EMBO journal* **26**, 2206-2217, doi:10.1038/sj.emboj.7601662 (2007).
733 8 Yi, C. & He, C. DNA repair by reversal of DNA damage. *Cold Spring Harbor perspectives in biology* **5**,
734 a012575, doi:10.1101/cshperspect.a012575 (2013).
735 9 Song, H. *et al.* METTL3 and ALKBH5 oppositely regulate m(6)A modification of TFEB mRNA, which
736 dictates the fate of hypoxia/reoxygenation-treated cardiomyocytes. *Autophagy* **15**, 1419-1437,
737 doi:10.1080/15548627.2019.1586246 (2019).
738 10 Chen, Z. *et al.* Psychological stress-induced ALKBH5 deficiency promotes tumour innervation and
739 pancreatic cancer via extracellular vesicle transfer of RNA. *Nat Cell Biol* **27**, 1035-1047,
740 doi:10.1038/s41556-025-01667-0 (2025).
741 11 Johannessen, T. C. *et al.* The DNA repair protein ALKBH2 mediates temozolomide resistance in human
742 glioblastoma cells. *Neuro Oncol* **15**, 269-278, doi:10.1093/neuonc/nos301 (2013).
743 12 Feng, S., Xu, Z., Peng, J. & Zhang, M. The AlkB Family: Potential Prognostic Biomarkers and Therapeutic
744 Targets in Glioblastoma. *Frontiers in oncology* **12**, 847821, doi:10.3389/fonc.2022.847821 (2022).
745 13 Wada, Y., Naito, T., Fukushima, T. & Saito, M. Evaluation of ALKBH2 and ALKBH3 gene regulation in
746 patients with adult T-cell leukemia/lymphoma. *Virology journal* **21**, 316, doi:10.1186/s12985-024-02590-w
747 (2024).
748 14 Dai, W. *et al.* Overcoming therapeutic resistance in oncolytic herpes virotherapy by targeting IGF2BP3-
749 induced NETosis in malignant glioma. *Nature communications* **15**, 131, doi:10.1038/s41467-023-44576-2
750 (2024).
751 15 Cui, Y. H. *et al.* Targeting DTX2/UFD1-mediated FTO degradation to regulate antitumor immunity.
752 *Proceedings of the National Academy of Sciences of the United States of America* **121**, e2407910121,
753 doi:10.1073/pnas.2407910121 (2024).
754 16 Liu, W. *et al.* TRIM17 promotes the progression of osteosarcoma by regulating PDK1 m6A modification-
755 mediated AKT/mTOR pathway activation through ubiquitination of FTO. *Cell death & disease* **16**, 767,
756 doi:10.1038/s41419-025-08070-5 (2025).

757 17 Han, T., Tong, W., Xie, J., Guo, X. & Zhang, L. FOXF2 suppressed esophageal squamous cell carcinoma by
758 reducing M2 TAMs via modulating RNF144A-FTO axis. *International immunopharmacology* **143**, 113422,
759 doi:10.1016/j.intimp.2024.113422 (2024).
760 18 Zhang, L. *et al.* FTO O-GlcNAcylation promotes TRIM21-mediated FTO ubiquitination degradation to
761 sustain the negative feedback control of macrophage inflammation. *Front Immunol* **16**, 1593243,
762 doi:10.3389/fimmu.2025.1593243 (2025).
763 19 Meng, S. *et al.* PRMT5-Mediated ALKBH5 Methylation Promotes Colorectal Cancer Immune Evasion via
764 Increasing CD276 Expression. *Research (Washington, D.C.)* **8**, 0549, doi:10.34133/research.0549 (2025).
765 20 Wang, K. *et al.* E3 ubiquitin ligase RNF180 mediates the ALKBH5/SMARCA5 axis to promote colon
766 inflammation and Th17/Treg imbalance in ulcerative colitis mice. *Archives of pharmacal research* **47**, 645-
767 658, doi:10.1007/s12272-024-01507-z (2024).
768 21 Lin, K. *et al.* m6A eraser FTO impairs gemcitabine resistance in pancreatic cancer through influencing
769 NEDD4 mRNA stability by regulating the PTEN/PI3K/AKT pathway. *J Exp Clin Cancer Res* **42**, 217,
770 doi:10.1186/s13046-023-02792-0 (2023).
771 22 Song, M. *et al.* USP18 Stabilized FTO Protein to Activate Mitophagy in Ischemic Stroke Through Repressing
772 m6A Modification of SIRT6. *Molecular neurobiology* **61**, 6658-6674, doi:10.1007/s12035-024-04001-1
773 (2024).
774 23 Zhou, X. *et al.* USP14 modulates stem-like properties, tumorigenicity, and radiotherapy resistance in
775 glioblastoma stem cells through stabilization of MST4-phosphorylated ALKBH5. *Theranostics* **15**, 2293-
776 2314, doi:10.7150/thno.103629 (2025).
777 24 Chang, G. *et al.* USP36 promotes tumorigenesis and drug sensitivity of glioblastoma by deubiquitinating and
778 stabilizing ALKBH5. *Neuro Oncol* **25**, 841-853, doi:10.1093/neuonc/noac238 (2023).
779 25 Duncan, T. *et al.* Reversal of DNA alkylation damage by two human dioxygenases. *Proceedings of the*
780 *National Academy of Sciences of the United States of America* **99**, 16660-16665,
781 doi:10.1073/pnas.262589799 (2002).
782 26 Ringvoll, J. *et al.* Repair deficient mice reveal mABH2 as the primary oxidative demethylase for repairing
783 1meA and 3meC lesions in DNA. *The EMBO journal* **25**, 2189-2198, doi:10.1038/sj.emboj.7601109 (2006).
784 27 Wang, P. *et al.* Oncometabolite D-2-Hydroxyglutarate Inhibits ALKBH DNA Repair Enzymes and Sensitizes
785 IDH Mutant Cells to Alkylating Agents. *Cell reports* **13**, 2353-2361, doi:10.1016/j.celrep.2015.11.029 (2015).
786 28 Li, Q. *et al.* Rhein Inhibits AlkB Repair Enzymes and Sensitizes Cells to Methylated DNA Damage. *J Biol*
787 *Chem* **291**, 11083-11093, doi:10.1074/jbc.M115.711895 (2016).
788 29 Wu, G. *et al.* ALKBH1-8 and FTO: Potential Therapeutic Targets and Prognostic Biomarkers in Lung
789 Adenocarcinoma Pathogenesis. *Frontiers in cell and developmental biology* **9**, 633927,
790 doi:10.3389/fcell.2021.633927 (2021).
791 30 Wu, S. S. *et al.* Down-regulation of ALKBH2 increases cisplatin sensitivity in H1299 lung cancer cells. *Acta*
792 *pharmacologica Sinica* **32**, 393-398, doi:10.1038/aps.2010.216 (2011).
793 31 Xu, L. *et al.* Boosting cisplatin chemotherapy by nanomotor-enhanced tumor penetration and DNA adducts
794 formation. *Journal of nanobiotechnology* **20**, 429, doi:10.1186/s12951-022-01622-3 (2022).
795 32 Li, X. *et al.* An integrated LC-MS/MS platform for noninvasive urinary nucleus acid adductomics: A pilot
796 study for tobacco exposure. *Journal of hazardous materials* **474**, 134780,
797 doi:10.1016/j.jhazmat.2024.134780 (2024).

33 Hegi, M. E. *et al.* MGMT gene silencing and benefit from temozolomide in glioblastoma. *The New England journal of medicine* **352**, 997-1003, doi:10.1056/NEJMoa043331 (2005).

34 Wilson, D. L., Beharry, A. A., Srivastava, A., O'Connor, T. R. & Kool, E. T. Fluorescence Probes for ALKBH2 Allow the Measurement of DNA Alkylation Repair and Drug Resistance Responses. *Angewandte Chemie (International ed. in English)* **57**, 12896-12900, doi:10.1002/anie.201807593 (2018).

35 Brickner, J. R. *et al.* A ubiquitin-dependent signalling axis specific for ALKBH-mediated DNA dealkylation repair. *Nature* **551**, 389-393, doi:10.1038/nature24484 (2017).

36 Hatakeyama, S. TRIM proteins and cancer. *Nat Rev Cancer* **11**, 792-804, doi:10.1038/nrc3139 (2011).

37 Gu, J., Chen, J., Xiang, S., Zhou, X. & Li, J. Intricate confrontation: Research progress and application potential of TRIM family proteins in tumor immune escape. *Journal of advanced research* **54**, 147-179, doi:10.1016/j.jare.2023.01.011 (2023).

38 Dudley-Fraser, J. *et al.* Identification of RING E3 pseudoligases in the TRIM protein family. *Nature communications* **16**, 3456, doi:10.1038/s41467-025-58807-1 (2025).

39 Randolph, K., Hyder, U. & D'Orso, I. KAP1/TRIM28: Transcriptional Activator and/or Repressor of Viral and Cellular Programs? *Frontiers in cellular and infection microbiology* **12**, 834636, doi:10.3389/fcimb.2022.834636 (2022).

40 Czerwińska, P., Mazurek, S. & Wiznerowicz, M. The complexity of TRIM28 contribution to cancer. *Journal of biomedical science* **24**, 63, doi:10.1186/s12929-017-0374-4 (2017).

41 Yalçin, Z. *et al.* UBE2D3 facilitates NHEJ by orchestrating ATM signalling through multi-level control of RNF168. *Nature communications* **15**, 5032, doi:10.1038/s41467-024-49431-6 (2024).

42 Goodarzi, A. A., Kurka, T. & Jeggo, P. A. KAP-1 phosphorylation regulates CHD3 nucleosome remodeling during the DNA double-strand break response. *Nature structural & molecular biology* **18**, 831-839, doi:10.1038/nsmb.2077 (2011).

43 Yang, Y. *et al.* HIF-1 Interacts with TRIM28 and DNA-PK to release paused RNA polymerase II and activate target gene transcription in response to hypoxia. *Nature communications* **13**, 316, doi:10.1038/s41467-021-27944-8 (2022).

44 Li, Y., Xie, H., Liu, S., Ruan, Z. & Wang, B. Resveratrol Alleviates Ischemia-Reperfusion-Induced Neuronal Damage by Inhibiting NR3C2-Mediated TRIM28 Expression. *Journal of integrative neuroscience* **24**, 31375, doi:10.31083/jin31375 (2025).

45 Wang, Z. *et al.* FOXA1-dependent NSUN2 facilitates the advancement of prostate cancer by preserving TRIM28 mRNA stability in a m5C-dependent manner. *NPJ precision oncology* **9**, 127, doi:10.1038/s41698-025-00904-x (2025).

46 Jana, S. *et al.* PITAR, a DNA damage-inducible cancer/testis long noncoding RNA, inactivates p53 by binding and stabilizing TRIM28 mRNA. *eLife* **12**, doi:10.7554/eLife.88256 (2024).

47 Chen, Y. *et al.* March5-mediated Trim28 degradation preserves islet β-cell function in mice. *Nature communications* **16**, 7073, doi:10.1038/s41467-025-62587-z (2025).

48 Kuo, C. Y. *et al.* An arginine-rich motif of ring finger protein 4 (RNF4) oversees the recruitment and degradation of the phosphorylated and SUMOylated Krüppel-associated box domain-associated protein 1 (KAP1)/TRIM28 protein during genotoxic stress. *J Biol Chem* **289**, 20757-20772, doi:10.1074/jbc.M114.555672 (2014).

49 Xiao, T. Z., Suh, Y. & Longley, B. J. MAGE proteins regulate KRAB zinc finger transcription factors and

KAP1 E3 ligase activity. *Archives of biochemistry and biophysics* **563**, 136-144, doi:10.1016/j.abb.2014.07.026 (2014).

50 Doyle, J. M., Gao, J., Wang, J., Yang, M. & Potts, P. R. MAGE-RING protein complexes comprise a family of E3 ubiquitin ligases. *Molecular cell* **39**, 963-974, doi:10.1016/j.molcel.2010.08.029 (2010).

51 Li, K. *et al.* Development of Ligands and Degraders Targeting MAGE-A3. *Journal of the American Chemical Society* **146**, 24884-24891, doi:10.1021/jacs.4c05393 (2024).

52 Yang, C. G. *et al.* Crystal structures of DNA/RNA repair enzymes AlkB and ABH2 bound to dsDNA. *Nature* **452**, 961-965, doi:10.1038/nature06889 (2008).

53 Le, H. P. *et al.* DSS1 and ssDNA regulate oligomerization of BRCA2. *Nucleic acids research* **48**, 7818-7833, doi:10.1093/nar/gkaa555 (2020).

54 Gu, P., Deng, W., Lei, M. & Chang, S. Single strand DNA binding proteins 1 and 2 protect newly replicated telomeres. *Cell research* **23**, 705-719, doi:10.1038/cr.2013.31 (2013).

55 Feng, Y., Gao, J. & Yang, M. When MAGE meets RING: insights into biological functions of MAGE proteins. *Protein Cell* **2**, 7-12, doi:10.1007/s13238-011-1002-9 (2011).

56 Pineda, C. T. *et al.* Degradation of AMPK by a cancer-specific ubiquitin ligase. *Cell* **160**, 715-728, doi:10.1016/j.cell.2015.01.034 (2015).

57 Tsang, Y. H. *et al.* Differential expression of MAGEA6 toggles autophagy to promote pancreatic cancer progression. *eLife* **9**, doi:10.7554/eLife.48963 (2020).

58 Zhao, W. *et al.* CTT1 overexpression increases the replicative lifespan of MMS-sensitive Saccharomyces cerevisiae deficient in KSP1. *Mechanisms of ageing and development* **164**, 27-36, doi:10.1016/j.mad.2017.03.008 (2017).

59 Bu, X. *et al.* CD147 confers temozolomide resistance of glioma cells via the regulation of β-TrCP/Nrf2 pathway. *International journal of biological sciences* **17**, 3013-3023, doi:10.7150/ijbs.60894 (2021).

60 Lombard, D. B. *et al.* High-throughput small molecule screening reveals Nrf2-dependent and -independent pathways of cellular stress resistance. *Science advances* **6**, doi:10.1126/sciadv.aaz7628 (2020).

61 Lee, D. H. *et al.* Repair of methylation damage in DNA and RNA by mammalian AlkB homologues. *J Biol Chem* **280**, 39448-39459, doi:10.1074/jbc.M509881200 (2005).

62 Ivanov, A. V. *et al.* PHD domain-mediated E3 ligase activity directs intramolecular sumoylation of an adjacent bromodomain required for gene silencing. *Molecular cell* **28**, 823-837, doi:10.1016/j.molcel.2007.11.012 (2007).

63 Prince, C. *et al.* Investigating the impact of cigarette smoking behaviours on DNA methylation patterns in adolescence. *Hum Mol Genet* **28**, 155-165, doi:10.1093/hmg/ddy316 (2019).

64 Tan, Q. *et al.* miR-125b-5p upregulation by TRIM28 induces cisplatin resistance in non-small cell lung cancer through CREB1 inhibition. *BMC pulmonary medicine* **22**, 469, doi:10.1186/s12890-022-02272-9 (2022).

65 Kim, H. J. *et al.* Roles of NADPH oxidases in cisplatin-induced reactive oxygen species generation and ototoxicity. *The Journal of neuroscience : the official journal of the Society for Neuroscience* **30**, 3933-3946, doi:10.1523/jneurosci.6054-09.2010 (2010).

66 Xu, G. L. & Bochtler, M. Reversal of nucleobase methylation by dioxygenases. *Nature chemical biology* **16**, 1160-1169, doi:10.1038/s41589-020-00675-5 (2020).

67 Pineda, C. T. & Potts, P. R. Oncogenic MAGEA-TRIM28 ubiquitin ligase downregulates autophagy by

880 ubiquitinating and degrading AMPK in cancer. *Autophagy* **11**, 844-846,
881 doi:10.1080/15548627.2015.1034420 (2015).
882 68 Jin, X. *et al.* MAGE-TRIM28 complex promotes the Warburg effect and hepatocellular carcinoma
883 progression by targeting FBP1 for degradation. *Oncogenesis* **6**, e312, doi:10.1038/oncsis.2017.21 (2017).
884 69 Malacrida, A. *et al.* MV1035 Overcomes Temozolomide Resistance in Patient-Derived Glioblastoma Stem
885 Cell Lines. *Biology* **11**, doi:10.3390/biology11010070 (2022).
886 70 Ke, B., Ye, K. & Cheng, S. ALKBH2 inhibition alleviates malignancy in colorectal cancer by regulating
887 BMI1-mediated activation of NF-κB pathway. *World journal of surgical oncology* **18**, 328,
888 doi:10.1186/s12957-020-02106-0 (2020).
889 71 Lin, J. R., Zeman, M. K., Chen, J. Y., Yee, M. C. & Cimprich, K. A. SHPRH and HLTF act in a damage-
890 specific manner to coordinate different forms of postreplication repair and prevent mutagenesis. *Molecular*
891 *cell* **42**, 237-249, doi:10.1016/j.molcel.2011.02.026 (2011).
892 72 Tsao, N. *et al.* Aberrant RNA methylation triggers recruitment of an alkylation repair complex. *Molecular*
893 *cell* **81**, 4228-4242.e4228, doi:10.1016/j.molcel.2021.09.024 (2021).
894 73 Fong, K. W., Zhao, J. C., Song, B., Zheng, B. & Yu, J. TRIM28 protects TRIM24 from SPOP-mediated
895 degradation and promotes prostate cancer progression. *Nature communications* **9**, 5007, doi:10.1038/s41467-
896 018-07475-5 (2018).
897 74 Herquel, B. *et al.* Transcription cofactors TRIM24, TRIM28, and TRIM33 associate to form regulatory
898 complexes that suppress murine hepatocellular carcinoma. *Proceedings of the National Academy of Sciences*
899 *of the United States of America* **108**, 8212-8217, doi:10.1073/pnas.1101544108 (2011).
900 75 Jaiswal, H. *et al.* ATM/Wip1 activities at chromatin control Plk1 re-activation to determine G2 checkpoint
901 duration. *The EMBO journal* **36**, 2161-2176, doi:10.15252/embj.201696082 (2017).
902 76 Wang, C. *et al.* MDM2 interaction with nuclear corepressor KAP1 contributes to p53 inactivation. *The EMBO*
903 *journal* **24**, 3279-3290, doi:10.1038/sj.emboj.7600791 (2005).
904 77 Hoang, T. T. *et al.* Comprehensive evaluation of smoking exposures and their interactions on DNA
905 methylation. *EBioMedicine* **100**, 104956, doi:10.1016/j.ebiom.2023.104956 (2024).
906 78 Liu, L. *et al.* TRIM28 knockdown increases sensitivity to etoposide by upregulating E2F1 in non-small cell
907 lung cancer. *Oncology reports* **37**, 3597-3605, doi:10.3892/or.2017.5638 (2017).
908 79 Ginn, L. *et al.* A TIAM1-TRIM28 complex mediates epigenetic silencing of protocadherins to promote
909 migration of lung cancer cells. *Proceedings of the National Academy of Sciences of the United States of*
910 *America* **120**, e2300489120, doi:10.1073/pnas.2300489120 (2023).
911 80 Saxena, T. *et al.* EGFR-induced lncRNA TRIDENT promotes drug resistance in non-small cell lung cancer
912 via phospho-TRIM28-mediated DNA damage repair. *Proceedings of the National Academy of Sciences of*
913 *the United States of America* **122**, e2415389122, doi:10.1073/pnas.2415389122 (2025).
914 81 Lundholm, L. *et al.* Resistance to DNA-damaging treatment in non-small cell lung cancer tumor-initiating
915 cells involves reduced DNA-PK/ATM activation and diminished cell cycle arrest. *Cell death & disease* **4**,
916 e478, doi:10.1038/cddis.2012.211 (2013).
917

## Figure legends

**Figure 1. TRIM28 directly binds ALKBH2. (A)** Silver staining and LC–MS/MS identification of ALKBH2 as a TRIM28-associated protein following affinity purification from H1299 NSCLC cells; the TRIM28 band is indicated. **(B)** Co-immunoprecipitation (co-IP) analysis of HEK293T cells co-expressing HA-ALKBH2 and Flag-TRIM28 or Flag-TRIM24; Flag IP was followed by western blotting (WB). Representative of two independent co-IP experiments with similar results. WB was repeated on the same IP samples to ensure signal consistency. **(C)** Reciprocal co-IP using HA-ALKBH2 and Flag-TRIM28 (or HA-GFP control), analyzed by HA IP. Representative of two independent experiments with similar results. **(D)** Schematic of full-length TRIM28 and truncation mutants. **(E)** Domain mapping using Flag IP in HEK293T cells co-transfected with HA-ALKBH2 and individual TRIM28 truncation constructs. Results were reproduced in independent experiments. **(F)** Endogenous ALKBH2–TRIM28 interaction detected by co-IP using an anti-TRIM28 antibody in H1299 cell lysates. Representative of two independent experiments. **(G)** Immunofluorescence (IF) showing nuclear co-localization of endogenous ALKBH2 (green) and TRIM28 (red); nuclei were counterstained with DAPI (blue). Scale bar, 20 μm. Pearson correlation coefficient (PCC) = 0.896 ± 0.016 (mean ± SD, N = 42 cells). **(H)** *In vitro* MBP pull-down assay using recombinant His-Flag-ALKBH2 and purified MBP-TRIM28. Representative of two independent experiments. **(I)** Specificity profiling of endogenous TRIM28 binding in HEK293T cells transfected with Flag-ALKBH2 or Flag-ALKBH3. Representative of two independent experiments with similar results. **(J)** GRAMM-X docking of TRIM28 RBCC (cyan) with ALKBH2 (light red) or ALKBH3 (green). Middle panel: magnified interface highlighting the Finger and Long-loop motifs (red). Right panel: superposition with the ALKBH2–DNA structure (orange), showing partial overlap between TRIM28- and DNA-binding surfaces. **(K)** Flag IP of lysates from HEK293T cells expressing Flag-ALKBH2 in the presence of increasing ssDNA concentrations. Representative of two independent experiments with similar results. Source data are provided as a Source Data file.

**Figure 2. TRIM28 promotes K48-linked ubiquitination and proteasomal degradation of**

946 **ALKBH2. (A)** In vivo ubiquitination assay in HEK293T cells co-transfected with Flag-ALKBH2
947 and HA-ubiquitin (Ub), treated with MG132 (10 μM, 6 h). Lysates were subjected to denaturing
948 IP (1% SDS) followed by WB. N = 3 independent experiments. **(B)** Denaturing Flag IP in
949 HEK293T cells co-transfected with Flag-ALKBH2 and HA-tagged WT, K48-only, or K48R
950 ubiquitin. Representative of two independent experiments with similar results. **(C)** K48-linked
951 polyubiquitin enrichment using Halo-TUBE beads in HEK293T cells expressing Flag-ALKBH2
952 treated with MG132. Representative of two independent experiments with similar results. **(D)**
953 Denaturing Flag IP in HEK293T cells co-transfected with Flag-ALKBH2, His-TRIM28, and HA-
954 K48-only ubiquitin. Representative of two independent experiments with similar results. **(E)**
955 Analysis of ALKBH2 ubiquitination in HEK293T cells co-transfected with Flag-ALKBH2 and
956 WT or RING-inactive (C65/68A) His-TRIM28. Representative of two independent experiments.
957 **(F)** Denaturing Flag IP assessing K48-linked ALKBH2 ubiquitination in TRIM28-knockdown
958 HEK293T cells reconstituted with shRNA-resistant TRIM28. Representative of two independent
959 experiments. **(G)** WB analysis of H1299 and A549 cells transduced with control (shCon) or
960 TRIM28 shRNAs. N = 3 independent experiments. **(H)** qRT-PCR quantification of ALKBH2
961 mRNA in H1299 cells after TRIM28 depletion. Data points are shown as technical replicates (N =
962 4); experiments were independently repeated twice with similar results. **(I)** WB analysis of
963 ALKBH2 levels in H1299 and HEK293T cells overexpressing graded doses of TRIM28. N = 3
964 independent repeats. **(J)** WB analysis of H1299 cells transduced with control or ALKBH2 shRNAs.
965 N = 3 independent experiments. **(K)** WB analysis of ALKBH2-depleted H1299 cells reconstituted
966 with Flag-ALKBH2. N = 3 independent repeats. **(L)** qRT-PCR of TRIM28 transcript levels in
967 H1299 cells expressing empty vector or Flag-ALKBH2 (N = 4). Data were obtained using the
968 same replication scheme as in (H). Error bars indicate mean ± SD. Statistical comparisons were
969 performed using unpaired two-tailed Student's *t*-tests; NS, not significant. Source data are
970 provided as a Source Data file.
971
972 **Figure 3. MAGEA6 enhances the TRIM28–ALKBH2 interaction and promotes ALKBH2**

973 **degradation. (A)** Flag IP analysis of the interaction between Myc-MAGEA6 and Flag-ALKBH2
974 (or GFP control) in HEK293T cells. Representative of two independent experiments with similar
975 results. **(B)** *In vitro* pull-down assay using recombinant His-Flag-ALKBH2 and purified MBP-
976 MAGEA6. Representative of two independent experiments. **(C)** Flag IP in HEK293T cells (±
977 TRIM28 knockdown) co-transfected with HA-ALKBH2 and Flag-MAGEA6. Representative of
978 two independent experiments. **(D)** Flag IP analysis of the ALKBH2–TRIM28 interaction in
979 HEK293T cells transfected with Myc-MAGEA6. Representative of two independent experiments.
980 **(E)** HA IP in H1299 cells stably expressing HA-ALKBH2 following MAGEA3/6 knockdown with
981 shMAGEA3/6#1 or shMAGEA3/6#2. Representative of two independent experiments with
982 similar results. **(F)** Halo-TUBE pull-down in TRIM28-knockdown HEK293T cells overexpressing
983 Myc-MAGEA6. Representative of two independent experiments. **(G)** WB analysis of ALKBH2
984 stability in sgControl or TRIM28-knockout (sgTRIM28) H1299 cells transfected with MAGEA6
985 and treated with cycloheximide (CHX, 150 μg/mL). **(H)** Quantification of ALKBH2 protein levels
986 from (G). Data were quantified from 3 biological replicates (N = 3). **(I)** Flag IP mapping
987 interactions between Flag-MAGEA6 (WT or mutants), endogenous TRIM28, and co-expressed
988 HA-ALKBH2 in HEK293T cells. Representative of two independent experiments. **(J)** Halo-TUBE
989 pull-down of ubiquitinated proteins in HEK293T cells co-expressing HA-ALKBH2 and Flag-
990 MAGEA6 (WT or mutants). Representative of two independent experiments with similar results.
991 **(K)** Flag IP of HEK293T cells transfected with HA-ALKBH2 and cancer-associated Flag-
992 MAGEA6 mutants. Representative of two independent experiments. Error bars indicate mean ±
993 SD. Statistical comparisons were performed using unpaired two-tailed Student's *t*-tests. NS, not
994 significant. Source data are provided as a Source Data file.
995
996 **Figure 4. MMS dynamically regulates the TRIM28–ALKBH2 pathway. (A)** Flag IP from
997 H1299 cells expressing HA-ALKBH2 and Flag-TRIM28 treated with MMS (100 μM) and MG132
998 (10 μM) for the indicated times. Representative of two independent experiments with similar
999 results. **(B)** Flag IP from H1299 cells expressing Flag-TRIM28 treated with the indicated MMS

1000 concentrations (3 h, +MG132). Representative of two independent experiments. **(C)** WB analysis
1001 of MAGEA3/6 in nuclear and cytoplasmic fractions of H1299 cells treated with MMS (100 μM,
1002 4 h). Representative of two independent experiments. **(D)** Flag IP of H1299 cells expressing Flag-
1003 ALKBH2 treated with MMS (0–200 μM, 3 h) plus MG132. Representative of two independent
1004 experiments with similar results. **(E)** Degradation assay in H1299 cells expressing TAP-ALKBH2
1005 transduced with Flag-TRIM28 or vector and treated with MMS (100 μM). N = 3 independent
1006 repeats. **(F)** Flag IP of cell lysates incubated with ssDNA (1 μM), $H_2O_2$ (200 μM), ascorbate (Vc,
1007 500 μM), or EDTA (5 mM). Representative of two independent experiments with similar results.
1008 **(G)** Flag IP assessing the effect of EDTA (5 mM) on $H_2O_2$-induced interactions in ssDNA-
1009 containing lysates. Representative of two independent experiments. **(H)** Halo-TUBE pull-down in
1010 H1299 cells expressing TAP-ALKBH2 treated with MG132 (10 μM), MMS (100 μM), and Vc
1011 (500 μM) for 8 h. Representative of two independent experiments with similar results. **(I)** WB
1012 analysis of ALKBH2 in H1299 and H460 cells treated with MMS (100 μM). **(J)** Quantification of
1013 ALKBH2 protein levels from (I). Data were quantified from 4 biological replicates (N = 4). **(K)**
1014 WB analysis of H1299 cells expressing HA-TRIM28 treated with MMS (100 μM). N = 3
1015 independent experiments. **(L)** qRT-PCR of ALKBH2 in H1299 cells treated with MMS (100 μM).
1016 Data points are shown as technical replicates (N = 4); experiments were independently repeated
1017 twice with similar results. Error bars indicate mean ± SD. Statistical comparisons were performed
1018 using unpaired two-tailed Student's *t*-tests. Source data are provided as a Source Data file.
1019

1020 **Figure 5. MMS induces K48-linked ubiquitination and proteasomal degradation of TRIM28.**
1021 **(A, B)** WB analysis of TRIM28 levels in H1299 cells treated with MMS in a time-dependent (A)
1022 or dose-dependent (B) manner. N = 3 independent experiments. **(C)** qRT-PCR of TRIM28 mRNA
1023 in cells treated with MMS (100 μM). Data points are shown as technical replicates (N = 4);
1024 experiments were independently repeated twice with similar results. **(D)** Denaturing Flag IP of
1025 HEK293T cells expressing Flag-TRIM28 and HA-Ub treated with MMS and MG132 (10 μM).
1026 Representative of two independent experiments with similar results. **(E)** Flag IP and K48-specific

1027 ubiquitin WB in H1299 cells expressing Flag-TRIM28 treated with MMS (100 μM) + MG132.
1028 Representative of two independent experiments with similar results. **(F)** Denaturing Flag IP in
1029 HEK293T cells transfected with Flag-TRIM28 and HA-Ub (K48-only) treated with MMS (100
1030 μM). Representative of two independent experiments. **(G)** Halo-TUBE pull-down of endogenous
1031 TRIM28 in H1299 cells treated with MG132 and increasing MMS. Representative of two
1032 independent experiments. **(H)** Halo-TUBE pull-down comparing the effects of MMS (200 μM),
1033 temozolomide (TMZ, 200 μM), cisplatin (CDDP, 20 μM), or $H_2O_2$ (300 μM) on TRIM28
1034 ubiquitination (+MG132, 6 h). Representative of two independent experiments with similar results.
1035 **(I)** Halo-TUBE pull-down in HEK293T cells expressing Flag-TRIM28 WT or the SUMO-
1036 deficient mutant (K554/779/804R) treated with MMS. Representative of two independent
1037 experiments. **(J)** Flag IP in H1299 cells expressing Flag-TRIM28 treated with MMS (100 μM) +
1038 MG132. Representative of two independent experiments. **(K)** Flag IP in HEK293T cells
1039 expressing Flag-TRIM28 and Myc-MAGEA6 treated with MMS. Representative of two
1040 independent experiments. **(L)** Flag IP and WB in HEK293T cells expressing Flag-TRIM24 treated
1041 with MMS + MG132. Results were reproduced in independent experiments. **(M)** Halo-TUBE
1042 enrichment of K48-linked proteins in HEK293T cells overexpressing Flag-TRIM24 treated with
1043 MMS. Representative of two independent experiments with similar results. Error bars indicate
1044 mean ± SD. Statistical comparisons were performed using unpaired two-tailed Student's *t*-tests.
1045 NS, not significant. Source data are provided as a Source Data file.
1046
1047 **Figure 6. The TRIM28–ALKBH2 axis is clinically relevant and regulates sensitivity to**
1048 **alkylation damage. (A)** Relative mRNA expression of ALKBH2, ALKBH3, and MGMT in
1049 LUAD versus normal lung (TCGA dataset; Mann–Whitney test). **(B)** Representative ALKBH2
1050 IHC staining in LUAD and matched normal lung (Human Protein Atlas). Scale bar = 100 μm. **(C)**
1051 WB analysis of ALKBH2, TRIM28, ALKBH3, and MGMT in NSCLC cell lines and BEAS-2B
1052 cells. N = 3 independent experiments. **(D, E)** Kaplan–Meier overall survival of LUAD patients
1053 stratified by ALKBH2 (D) or ALKBH3 (E) mRNA expression. **(F)** CCK-8 proliferation assay in

1054 H1299 cells following ALKBH2 knockdown. **(G)** CCK-8 viability assay in H1299 cells with
1055 ALKBH2 knockdown, measured 48 h after a 1 h MMS pulse. **(H)** CCK-8 viability assay in H1299
1056 cells overexpressing Flag-TRIM28 WT or the RING-inactive mutant (C65/68A) after MMS pulse.
1057 **(I)** MMS sensitivity assessment in H1299 cells with TRIM28 knockdown and rescue. **(J)** Rescue
1058 of MMS hypersensitivity in H1299 cells by ALKBH2 co-expression. **(K)** Effect of MAGEA6
1059 overexpression on MMS cytotoxicity. **(L)** Effect of the TRIM28-binding–deficient MAGEA6
1060 mutant (D156E/S157Y) on MMS sensitivity. Data points are shown for panels F–L. For panels F,
1061 G, H, I, J, and L, data points represent four technical replicates from one representative experiment;
1062 the experiment was repeated twice with similar results. Panel K contains three technical replicates
1063 and was also repeated twice with similar results. Error bars indicate mean ± SD. Statistical
1064 comparisons were performed using unpaired two-tailed Student's *t*-tests or Mann–Whitney tests
1065 where appropriate. NS, not significant. Source data are provided as a Source Data file.
1066

1067 **Figure 7. Combining MMS with CDDP synergistically enhances cancer cell killing. (A)** CCK-
1068 8 viability assay of H1299 cells with TRIM28 knockdown treated with continuous low-dose MMS
1069 (48 h). **(B, C)** Colony formation assay of H460 cells overexpressing TRIM28 treated with MMS
1070 (100 μM) for 48 h, followed by drug removal and a 7-day growth period; representative images
1071 (B) and quantification (C). Colony numbers were averaged from 3 plates per experiment (N = 3),
1072 and the assay was repeated twice with similar results. **(D)** CCK-8 assay of H1299 cells
1073 overexpressing TRIM28 treated with MMS ± 2 μM CDDP. **(E)** CCK-8 assay of H1299 cells with
1074 ALKBH2 knockdown rescued by Flag-ALKBH2 and treated with MMS ± 2 μM CDDP. **(F)**
1075 Alkaline comet assay of H1299 cells treated with MMS (50 μM) and/or CDDP (2 μM); tail
1076 moments were quantified from 70 cells. The experiment was repeated twice with similar results.
1077 **(G, H)** $IC_{50}$ analysis of CDDP in H1299 (F) and H460 (G) cells with MMS co-treatment. **(I)**
1078 Representative images of clonogenic survival of H460 cells treated with MMS (75 μM) and CDDP
1079 (2 μM), and **(J)** colony quantification. Colony numbers were averaged from 3 plates per
1080 experiment (N = 3), and the assay was repeated twice with similar results. **(K, L)** 3D tumor

1081 spheroid growth of H1299 cells treated with MMS (100 μM) and CDDP (2 μM); Calcein-AM (live
1082 cells)/PI (dead cells) staining (K) and spheroid volume quantification (L). Data points represent
1083 individual spheroids from one representative experiment (n = 4 per condition); spheroid assays
1084 were independently repeated twice with similar results. Scale bar = 200 μm. For CCK-8 and $IC_{50}$
1085 assays (A, D, E, G, H), data points represent technical replicates from one representative
1086 experiment (three wells per condition, four wells in panel E); each experiment was independently
1087 repeated twice with similar results. Error bars indicate mean ± SD. Statistical comparisons were
1088 performed using unpaired two-tailed Student's *t*-tests; comet assay data in (E) were analyzed using
1089 the Mann–Whitney test. NS, not significant. Source data are provided as a Source Data file.
1090
1091 **Figure 8. Model of the biphasic TRIM28–ALKBH2 regulatory switch induced by alkylation**
1092 **stress. (I) Basal state.** MAGEA6-assisted, TRIM28-dependent K48-linked ubiquitination limits
1093 ALKBH2 at low basal levels, while ALKBH2 contributes to TRIM28 transcription. **(II) Acute**
1094 **MMS:** MMS increases TRIM28–ALKBH2 association, further enhanced by MAGEA6, and
1095 accelerates ALKBH2 degradation. **(III) Prolonged MMS:** Ubiquitination increasingly targets
1096 TRIM28, promoting its degradation and reducing ubiquitin-dependent suppression of ALKBH2.
1097 Combined with MMS-induced transcriptional activation of ALKBH2, this shift leads to a time-
1098 dependent increase in ALKBH2 levels.

Figure 1 (Sun et al.)

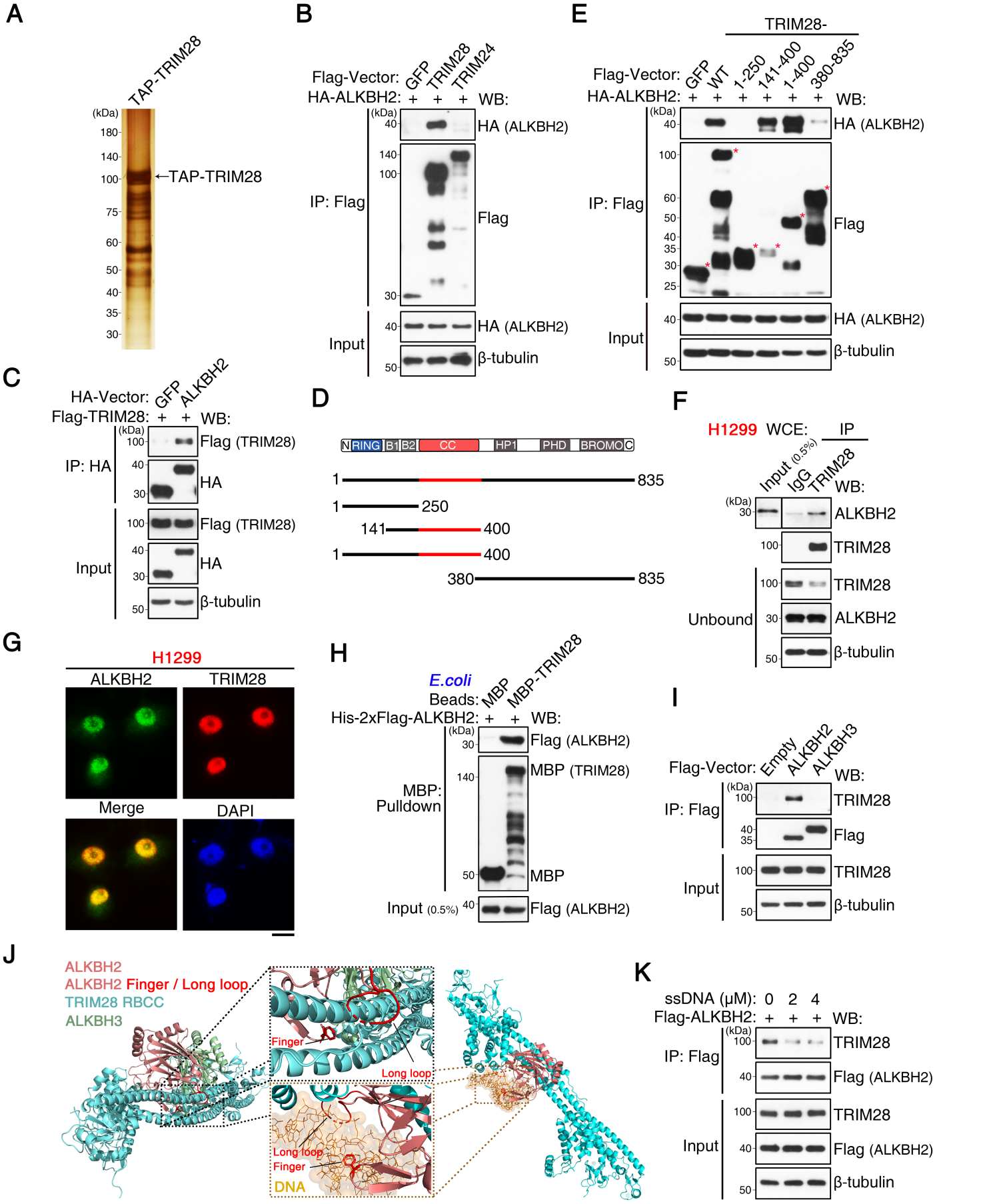

Figure 2 (Sun et al.)

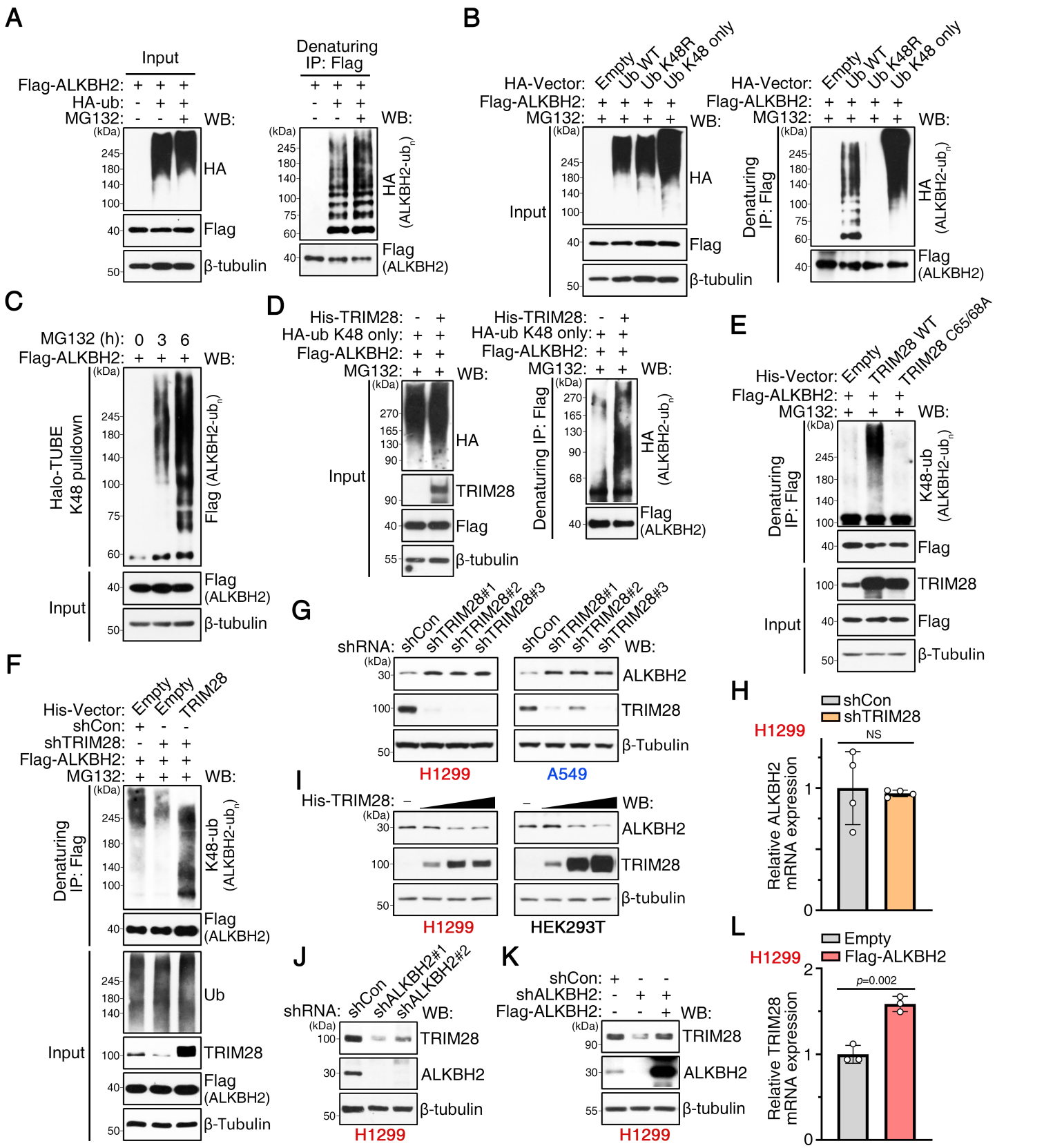

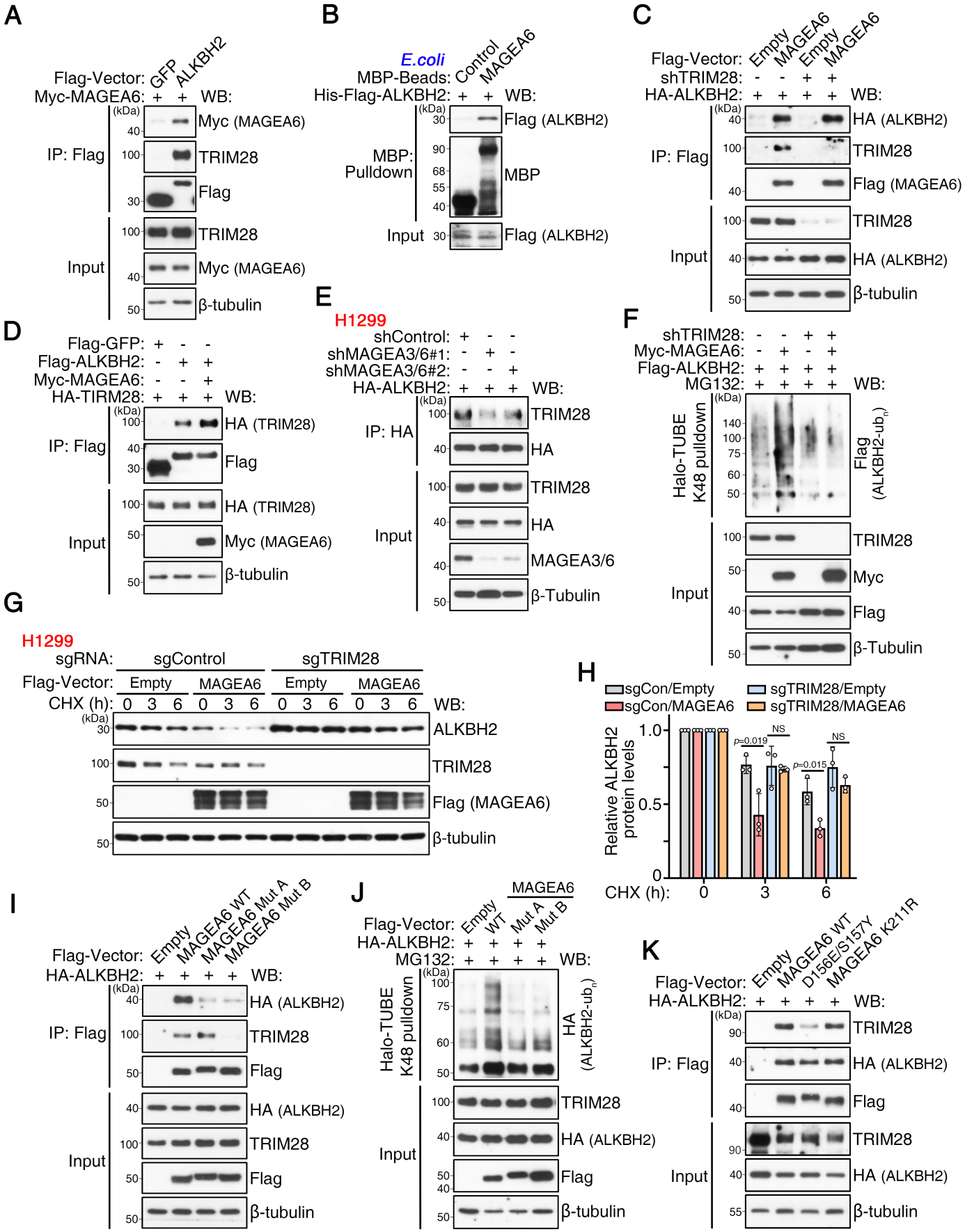
A
Flag-Vector: GFP ALKBH2
Myc-MAGEA6: + + WB:
IP: Flag
Input
Myc (MAGEA6)
TRIM28
Flag
β-tubulin
B
E.coli
MBP-Beads: Control MAGEA6
His-Flag-ALKBH2: + + WB:
MBP: Pulldown
Input
Flag (ALKBH2)
MBP
C
Flag-Vector: Empty MAGEA6 Empty MAGEA6
shTRIM28: - - + +
HA-ALKBH2: + + + + WB:
HA (ALKBH2)
Flag (MAGEA6)
D
Flag-GFP: + - -
Flag-ALKBH2: - + +
Myc-MAGEA6: - - +
HA-TIRM28: + + + WB:
HA (TRIM28)
E
H1299
shControl: + - -
shMAGEA3/6#1: - + -
shMAGEA3/6#2: - - +
HA-ALKBH2: + + + WB:
IP: HA
HA
MAGEA3/6
β-Tubulin
F
shTRIM28: - - + +
Myc-MAGEA6: - + - +
Flag-ALKBH2: + + + +
MG132: + + + + WB:
Halo-TUBE K48 pulldown
Flag (ALKBH2-ub$_n$)
Myc
G
H1299
sgRNA: sgControl sgTRIM28
Flag-Vector: Empty MAGEA6 Empty MAGEA6
CHX (h): 0 3 6 0 3 6 0 3 6 0 3 6 WB:
ALKBH2
Flag (MAGEA6)
H
sgCon/Empty
sgCon/MAGEA6
sgTRIM28/Empty
sgTRIM28/MAGEA6
Relative ALKBH2 protein levels
p=0.019
NS
p=0.015
CHX (h): 0 3 6
I
Flag-Vector: Empty MAGEA6 WT MAGEA6 Mut A MAGEA6 Mut B
HA-ALKBH2: + + + + WB:
J
MAGEA6
Flag-Vector: Empty WT Mut A Mut B
HA-ALKBH2: + + + +
MG132: + + + + WB:
Halo-TUBE K48 pulldown
HA (ALKBH2-ub$_n$)
K
Flag-Vector: Empty MAGEA6 WT MAGEA6 D156E/S157Y MAGEA6 K211R
HA-ALKBH2: + + + + WB:

Figure 4 (Sun et al.)

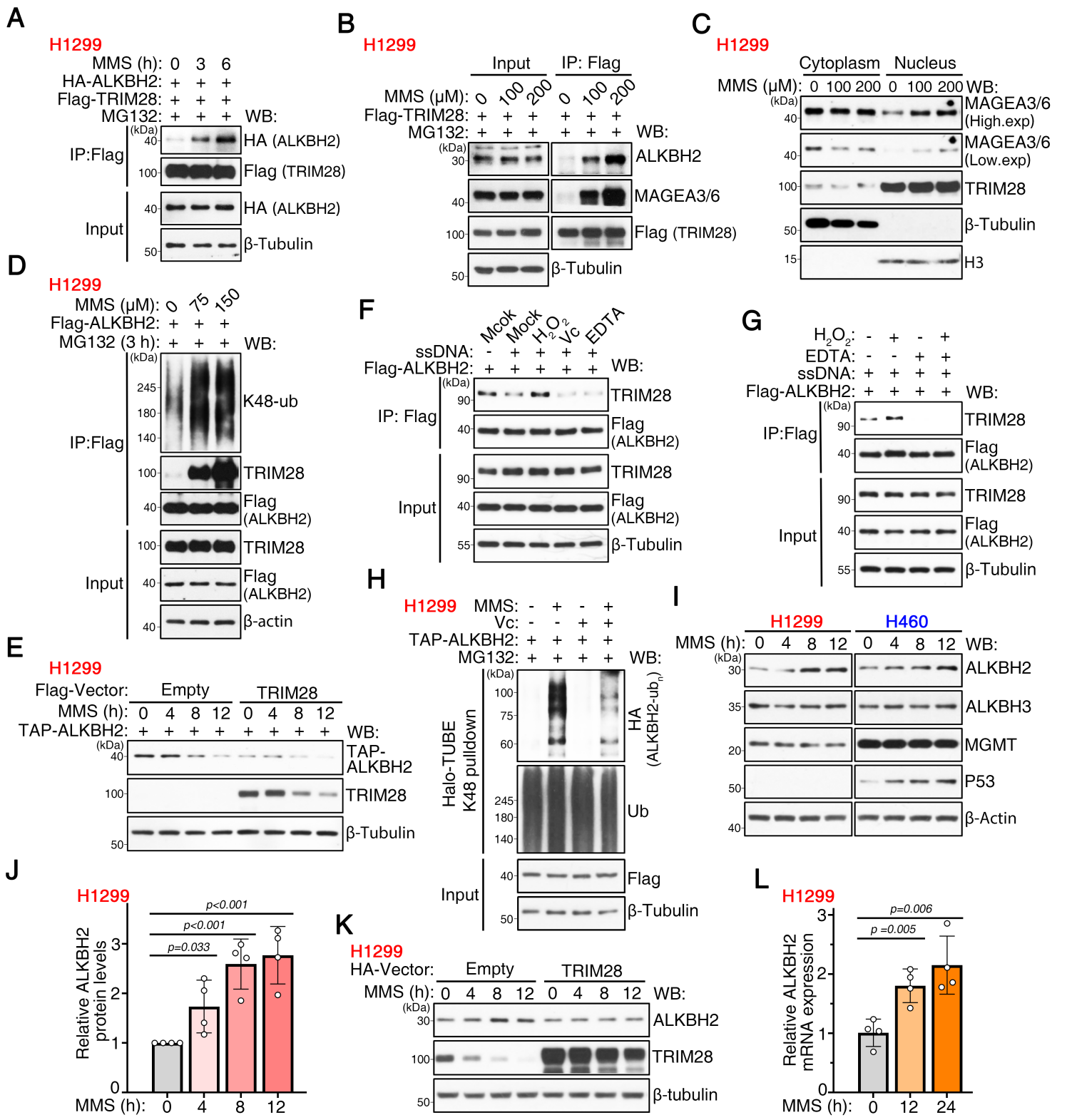

Figure 5 (Sun et al.)

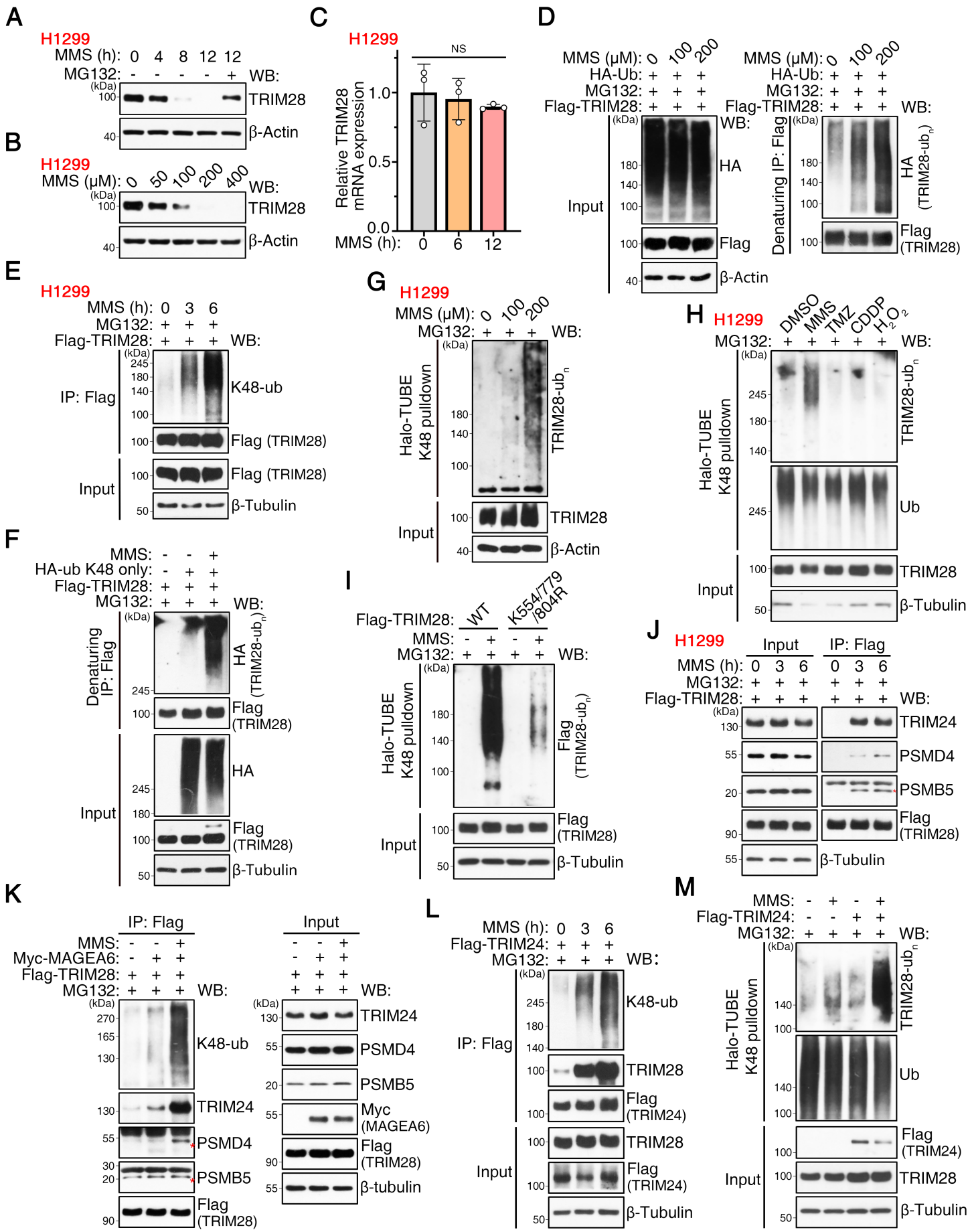

Figure 6 (Sun et al.)

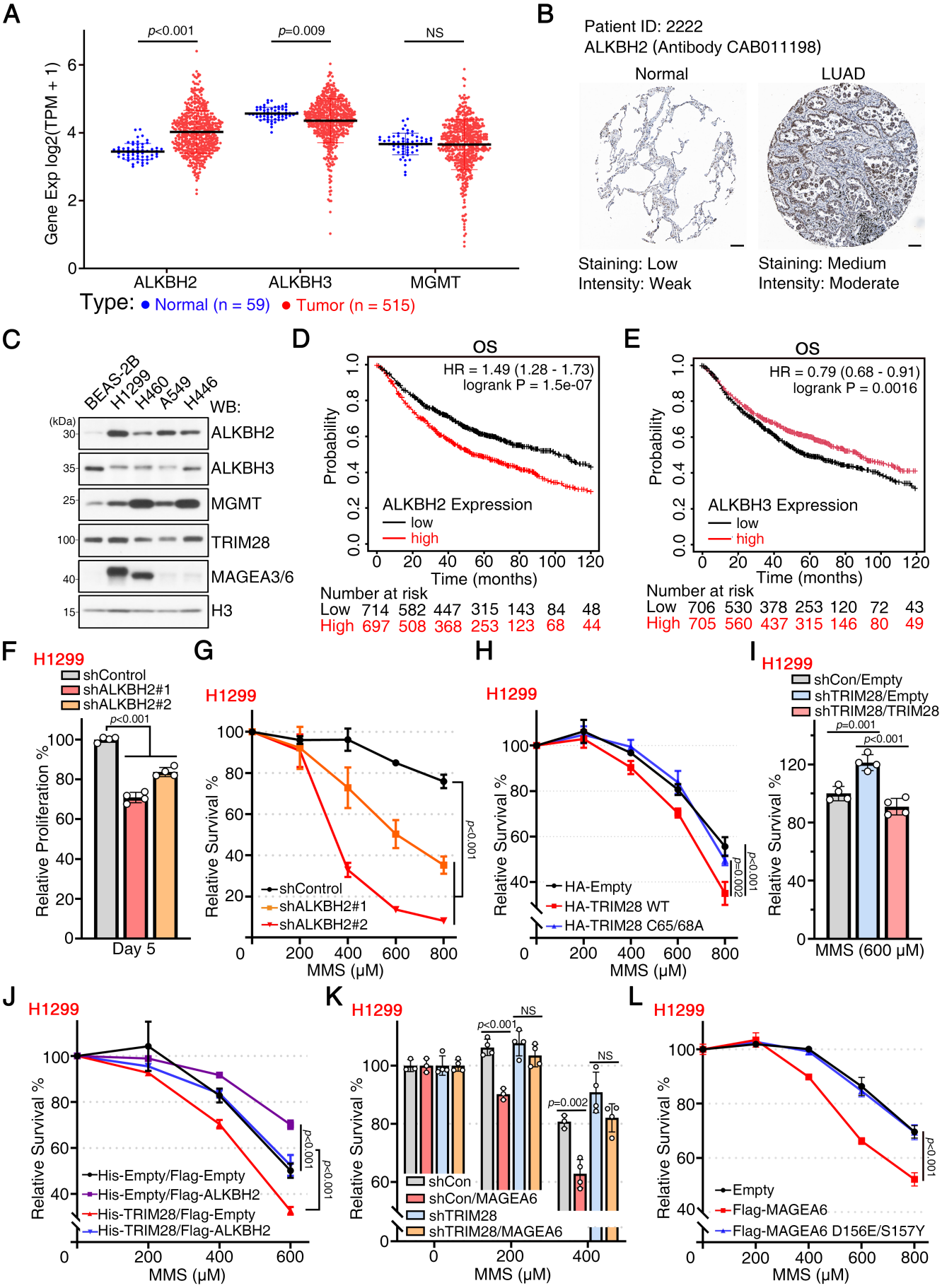

Figure 7 (Sun et al.)

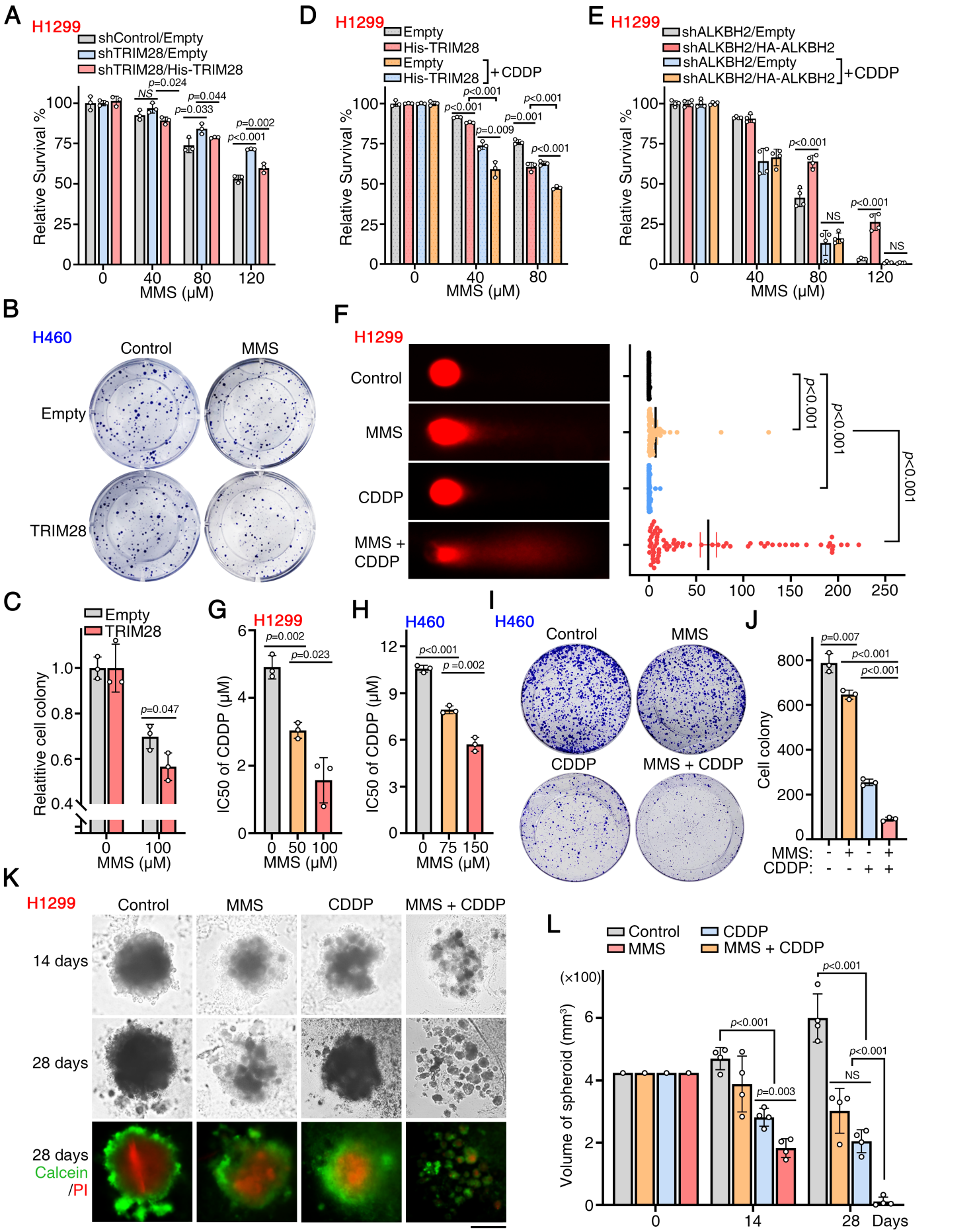
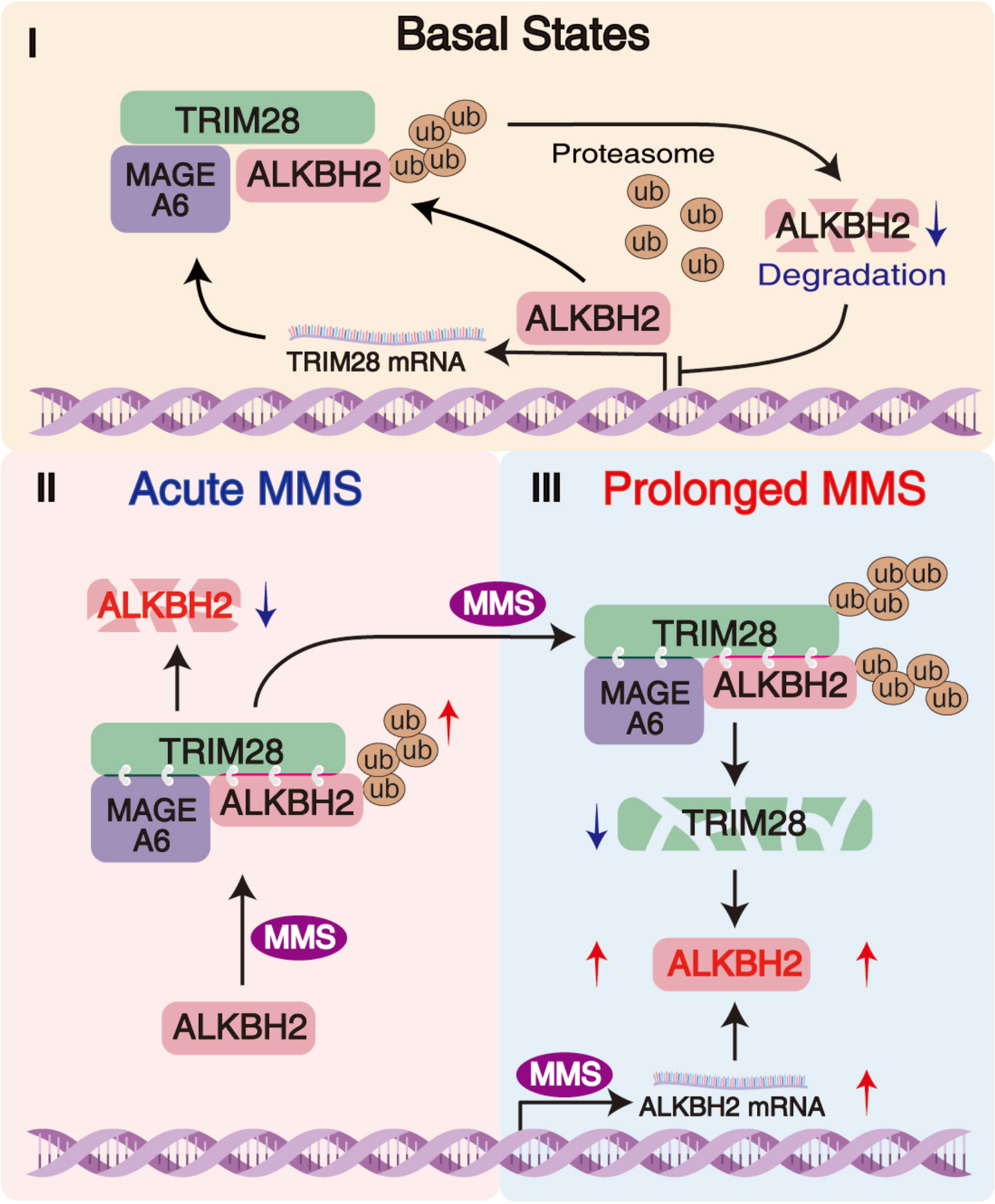
Figure 8 (Sun et al.)